# A comprehensive quantification of global nitrous oxide sources and sinks

Hanqin Tian[1], Rongting Xu[1], Josep G. Canadell[2], Rona L. Thompson[3], Wilfried Winiwarter[4,5], Parvadha Suntharalingam[6], Eric A. Davidson[7], Philippe Ciais[8], Robert B. Jackson[9,10,11], Greet Janssens-Maenhout[12,13], Michael J. Prather[14], Pierre Regnier[15], Naiqing Pan[1,16], Shufen Pan[1], Glen P. Peters[17], Hao Shi[1], Francesco N. Tubiello[18], Sönke Zaehle[19], Feng Zhou[20], Almut Arneth[21], Gianna Battaglia[22], Sarah Berthet[23], Laurent Bopp[24], Alexander F. Bouwman[25,26,27], Erik T. Buitenhuis[6,28], Jinfeng Chang[8,29], Martyn P. Chipperfield[30,31], Shree R. S. Dangal[32], Edward Dlugokencky[33], James W. Elkins[33], Bradley D. Eyre[34], Bojie Fu[16,35], Bradley Hall[33], Akihiko Ito[36], Fortunat Joos[22], Paul B. Krummel[37], Angela Landolfi[38,39], Goulven G. Laruelle[15], Ronny Lauerwald[8,15,40], Wei Li[8,41], Sebastian Lienert[22], Taylor Maavara[42], Michael MacLeod[43], Dylan B. Millet[44], Stefan Olin[45], Prabir K. Patra[46,47], Ronald G. Prinn[48], Peter A. Raymond[42], Daniel J. Ruiz[14], Guido R. van der Werf[49], Nicolas Vuichard[8], Junjie Wang[27], Ray F. Weiss[50], Kelley C. Wells[44], Chris Wilson[30,31], Jia Yang[51] & Yuanzhi Yao[1]

[1]International Center for Climate and Global Change Research, School of Forestry and Wildlife Sciences, Auburn University, Auburn, AL, USA
[2]Global Carbon Project, CSIRO Oceans and Atmosphere, Canberra, Australian Capital Territory, Australia
[3]Norsk Institutt for Luftforskning, NILU, Kjeller, Norway
[4]International Institute for Applied Systems Analysis, Laxenburg, Austria
[5] Institute of Environmental Engineering, University of Zielona Góra, Zielona Góra, Poland.
[6]School of Environmental Sciences, University of East Anglia, Norwich, UK
[7]Appalachian Laboratory, University of Maryland Center for Environmental Science, Frostburg, MD, USA
[8]Laboratoire des Sciences du Climat et de l'Environnement, LSCE, CEA CNRS, UVSQ UPSACLAY, Gif sur Yvette, France
[9]Department of Earth System Science, Stanford University, Stanford, CA, USA
[10]Woods Institute for the Environment, Stanford University, Stanford, CA, USA
[11]Precourt Institute for Energy, Stanford University, Stanford, CA, USA
[12]European Commission, Joint Research Centre (JRC), Ispra, Italy
[13]Ghent University, Faculty of Engineering and Architecture, Ghent, Belgium
[14]Department of Earth System Science, University of California Irvine, Irvine, CA, USA
[15]Department Geoscience, Environment & Society, Université Libre de Bruxelles, Brussels, Belgium
[16]State Key Laboratory of Urban and Regional Ecology, Research Center for Eco-Environmental Sciences, Chinese Academy of Sciences, Beijing, China
[17]CICERO Center for International Climate Research, Oslo, Norway
[18]Statistics Division, Food and Agriculture Organization of the United Nations, Via Terme di Caracalla, Rome, Italy
[19]Max Planck Institute for Biogeochemistry, Jena, Germany
[20]Sino-France Institute of Earth Systems Science, Laboratory for Earth Surface Processes, College of Urban and Environmental Sciences, Peking University, Beijing, China
[21]Karlsruhe Institute of Technology, Institute of Meteorology and Climate Research/Atmospheric Environmental Research, Garmisch-Partenkirchen, Germany

[22]Climate and Environmental Physics, Physics Institute and Oeschger Centre for Climate Change Research, University of Bern, Bern, Switzerland
[23]Centre National de Recherches Météorologiques (CNRM), Université de Toulouse, Météo-France, CNRS, Toulouse, France
[24]LMD-IPSL, Ecole Normale Supérieure / PSL Université, CNRS; Ecole Polytechnique, Sorbonne Université, Paris, France
[25]PBL Netherlands Environmental Assessment Agency, The Hague, The Netherlands
[26]Department of Earth Sciences – Geochemistry, Faculty of Geosciences, Utrecht University, Utrecht, The Netherlands
[27]Key Laboratory of Marine Chemistry Theory and Technology, Ministry of Education, Ocean University of China, Qingdao, China
[28]Tyndall Centre for Climate Change Research, School of Environmental Sciences, University of East Anglia, Norwich, UK
[29]College of Environmental and Resource Sciences, Zhejiang University, Hangzhou, China.
[30]National Centre for Earth Observation, University of Leeds, Leeds, UK
[31]Institute for Climate and Atmospheric Science, School of Earth and Environment, University of Leeds, Leeds, UK
[32]Woods Hole Research Center, Falmouth, MA, USA
[33]NOAA Global Monitoring Laboratory, Boulder, CO, USA
[34]Centre for Coastal Biogeochemistry, School of Environment Science and Engineering, Southern Cross University, Lismore, New South Wales, Australia
[35]Faculty of Geographical Science, Beijing Normal University, Beijing, China
[36]Center for Global Environmental Research, National Institute for Environmental Studies, Tsukuba, Japan
[37]Climate Science Centre, CSIRO Oceans and Atmosphere, Aspendale, Victoria, Australia
[38] GEOMAR Helmholtz Centre for Ocean Research Kiel, Kiel, Germany
[39]Istituto di Scienze Marine, Consiglio Nazionale delle Ricerche (CNR), Rome, Italy
[40]Université Paris-Saclay, INRAE, AgroParisTech, UMR ECOSYS, Thiverval-Grignon, France
[41]Ministry of Education Key Laboratory for Earth System modeling, Department of Earth System Science, Tsinghua University, Beijing, China
[42]Yale School of Forestry and Environmental Studies, New Haven, CT, USA
[43]Land Economy, Environment & Society, Scotland's Rural College (SRUC), Edinburgh, UK
[44]Department of Soil, Water, and Climate, University of Minnesota, St Paul, MN, USA
[45]Department of Physical Geography and Ecosystem Science, Lund University, Lund, Sweden
[46]Research Institute for Global Change, JAMSTEC, Yokohama, Japan
[47]Center for Environmental Remote Sensing, Chiba University, Chiba, Japan
[48]Center for Global Change Science, Massachusetts Institute of Technology, Cambridge, MA, USA
[49]Faculty of Science, Vrije Universiteit, Amsterdam, Netherlands.
[50] Scripps Institution of Oceanography, University of California San Diego, La Jolla, USA
[51]Department of Forestry, Mississippi State University, Mississippi State, MS, USA

**Nitrous oxide ($N_2O$), like carbon dioxide, is a long-lived greenhouse gas that accumulates in the atmosphere. The increase in atmospheric $N_2O$ concentrations over the past 150 years has contributed to stratospheric ozone depletion[1] and climate change[2]. Current national inventories do not provide a full picture of $N_2O$ emissions owing to their omission of natural sources and the limitations in methodology for attributing anthropogenic sources. In order to understand the steadily increasing atmospheric burden (about 2 percent per decade) and develop effective mitigation strategies, it is essential to improve quantification and attribution of natural and anthropogenic contributions and their uncertainties. Here we present a global $N_2O$ inventory that incorporates both natural and anthropogenic sources and accounts for the interaction between nitrogen additions and the biochemical processes that control $N_2O$ emissions. We use bottom-up (inventory; statistical extrapolation of flux measurements; process-based land and ocean modelling) and top-down (atmospheric inversion) approaches to provide a comprehensive quantification of global $N_2O$ sources and sinks resulting from 21 natural and human sectors between 1980 and 2016. Global $N_2O$ emissions were 17.0 (minimum-maximum: 12.2–23.5) teragrams of nitrogen per year (bottom-up) and 16.9 (15.9–17.7) teragrams of nitrogen per year (top-down) between 2007 and 2016. Global human-induced emissions, which are dominated by nitrogen additions to croplands, increased by 30% over the past four decades to 7.3 (4.2–11.4) teragrams of nitrogen per year. This increase was mainly responsible for the growth in the atmospheric burden. Our findings point to growing $N_2O$ emissions in emerging economies—particularly Brazil, China and India. Analysis of process-based model estimates reveals an emerging $N_2O$–climate feedback resulting from interactions between nitrogen additions and climate change. The recent growth in $N_2O$ emissions exceeds some**

**of the highest projected emission scenarios[3,4], underscoring the urgency to mitigate $N_2O$ emissions.**

Nitrous oxide ($N_2O$) is a long-lived stratospheric ozone-depleting substance and greenhouse gas (GHG) with a current atmospheric lifetime of 116±9 years (ref. [1]). The concentration of atmospheric $N_2O$ has increased by over 20% from 270 parts per billion (ppb) in 1750 to 331 ppb in 2018 (Extended Data Fig. 1), with the fastest growth observed in the past five decades[5,6]. Two key biochemical processes, nitrification and denitrification, control $N_2O$ production in both terrestrial and aquatic ecosystems, and are regulated by multiple environmental and biological factors, such as temperature, water, oxygen, acidity, substrate availability[7], particularly nitrogen (N) fertilizer use and livestock manure management, and recycling[8-10]. In the coming decades, $N_2O$ emissions are expected to continue increasing due to the growing demand for food, feed, fiber and energy, and a rising source from waste generation and industrial processes[4,11,12]. Since 1990, anthropogenic $N_2O$ emissions have been annually reported by Annex I Parties to the United Nations Framework Convention on Climate Change (UNFCCC). More recently, over 190 national signatories to the Paris Agreement are now required to report biannually their national GHG inventory with sufficient detail and transparency to track progress towards their Nationally Determined Contributions. Yet, these inventories do not provide a full picture of $N_2O$ emissions due to their omission of natural sources, the limitations in methodology for attributing anthropogenic sources, and missing data for a number of key regions (e.g., South America, Africa)[2,9,13]. Moreover, we need a complete account of all human activities that accelerate the global N cycle and that interact with the biochemical processes controlling the fluxes of $N_2O$ in both terrestrial and aquatic ecosystems[2,8]. Here we present a comprehensive, consistent analysis

and synthesis of the global $N_2O$ budget across all sectors, including natural and anthropogenic sources and sinks, using both bottom-up (BU) and top-down (TD) methods and their cross-constraints. Our assessment enhances understanding of the global N cycle and will inform policy development for $N_2O$ mitigation, ideally helping to curb warming to levels consistent with the long-term goal of the Paris Agreement.

A reconciling framework (described in Extended Data Fig. 2) was utilized to take full advantage of BU and TD approaches in estimating and constraining sources and sinks of $N_2O$. BU approaches include emission inventories, spatial extrapolation of field flux measurements, nutrient budget modeling, and process-based modeling for land and ocean fluxes. The TD approaches combine measurements of $N_2O$ mole fractions with atmospheric transport models in statistical optimization frameworks (inversions) to constrain the sources. Here we constructed a total of 43 flux estimates including 30 with BU approaches, five with TD approaches, and eight other estimates with observation and modeling approaches (see Methods; Extended Data Fig. 2).

With this extensive data and BU/TD framework, we establish the most comprehensive global and regional $N_2O$ budgets that include 18 sources and different versions of its chemical sink, which are further grouped into six categories (Fig. 1 and Table 1): 1) Natural sources (no anthropogenic effects) including a very small biogenic surface sink, 2) Perturbed fluxes from ecosystems induced by changes in climate, carbon dioxide ($CO_2$) and land cover, 3) Direct emissions of N additions in the agricultural sector (Agriculture), 4) Other direct anthropogenic sources, which include fossil fuel and industry, waste and waste water, and biomass burning, 5) Indirect emissions from ecosystems that are either downwind or downstream from the initial release of reactive N into the environment, which include $N_2O$ release following transport and deposition of anthropogenic N via the atmosphere or water bodies as defined by the

Intergovernmental Panel on Climate Change (IPCC)[14], and 6) The atmospheric chemical sink with one value derived from observations and the other (TD) from the inversion models. To quantify and attribute the regional $N_2O$ budget, we further partition the Earth's ice-free land into ten regions (Fig. 2 and Supplementary Fig. 1). With the construction of these budgets, we explore the relative temporal and spatial importance of multiple sources and sinks driving the atmospheric burden of $N_2O$, their uncertainties, and interactions between anthropogenic forcing and natural fluxes of $N_2O$ as an emerging climate feedback.

## The Global $N_2O$ Budget (2007–2016)

The BU and TD approaches give consistent estimates of global total $N_2O$ emissions in the recent decade to well within their respective uncertainties, with values of 17.0 (min-max: 12.2−23.5) Tg N $yr^{-1}$ and 16.9 (15.9−17.7) Tg N $yr^{-1}$ for BU and TD sources, respectively. The global calculated atmospheric chemical sink (i.e., $N_2O$ losses via photolysis and reaction with $O(^1D)$ in the troposphere and stratosphere) is 13.5 (12.4−14.6) Tg N $yr^{-1}$. The imbalance of sources and sinks of $N_2O$ derived from the averaged BU and TD estimates is 4.1 Tg N $yr^{-1}$. This imbalance agrees well with the observed 2007–2016 increase in atmospheric abundance of 3.8−4.8 Tg N $yr^{-1}$ (see Methods). Natural sources from soils and oceans contributed 57% of total emissions (mean: 9.7; min-max: 8.0−12.0 Tg N $yr^{-1}$) for the recent decade according to our BU estimate. We further estimate the natural soil flux at 5.6 (4.9−6.5) Tg N $yr^{-1}$ and the ocean flux at 3.4 (2.5−4.3) Tg N $yr^{-1}$ (see Methods).

Anthropogenic sources contributed on average 43% to the total $N_2O$ emission (mean: 7.3; min-max: 4.2−11.4 Tg N $yr^{-1}$), in which direct and indirect emissions from N additions in agriculture and other sectors contributed ~52% and ~18%, respectively. Of the remaining

anthropogenic emissions, ~27% were from other direct anthropogenic sources including fossil fuel and industry (~13%), with ~3% from perturbed fluxes caused by climate/$CO_2$/land cover change.

**Four Decades of the Global $N_2O$ Budget**

The atmospheric $N_2O$ burden increased from 1462 Tg N in the 1980s to 1555 Tg N in the recent decade, with a possible uncertainty ±20 Tg N. Our results (Table 1) demonstrate that global $N_2O$ emissions have also significantly increased, primarily driven by anthropogenic sources, with natural sources relatively steady throughout the study period. Our BU and TD global $N_2O$ emissions are comparable in magnitude during 1998–2016, but TD results imply a larger inter-annual variability (1.0 Tg N $yr^{-1}$; Extended Data Fig. 3a). BU and TD approaches diverge in the magnitude of land versus ocean emissions, although they are consistent with respect to trends. Specifically, the BU land estimate during 1998–2016 was on average 1.8 Tg N $yr^{-1}$ higher than the TD estimate, but showed a slightly slower increasing rate of 0.8±0.2 Tg N $yr^{-1}$ per decade (95% confidence interval; $P < 0.05$) compared to 1.1±0.6 Tg N $yr^{-1}$ per decade ($P < 0.05$) from TD (Extended Data Fig. 3b). Since 2005, the difference in the magnitude of emissions between the two approaches has become smaller due to a large TD-inferred emission increase, particularly in South America, Africa, and East Asia (Extended Data Fig. 3d, f, i). Oceanic $N_2O$ emissions from BU [3.6 (2.7–4.5) Tg N $yr^{-1}$] indicate a slight decline at a rate of 0.06 Tg N $yr^{-1}$ per decade ($P < 0.05$), while the TD approach gave a higher but stable value of 5.1 (3.4−7.1) Tg N $yr^{-1}$ during 1998–2016 (Table 1).

Based on BU approaches, anthropogenic $N_2O$ emissions increased from 5.6 (3.6−8.7) Tg N $yr^{-1}$ in the 1980s to 7.3 (4.2−11.4) Tg N $yr^{-1}$ in the recent decade at a rate of 0.6±0.2 Tg N $yr^{-1}$ per

decade ($P < 0.05$). Up to 87% of this increase is from direct emission from agriculture (71%) and indirect emission from anthropogenic N additions into soils (16%). Direct soil emission from fertilizer applications is the major source for agricultural emission increases, followed by a small but significant increase in emissions from livestock manure and aquaculture. The model-based estimates of direct soil emissions[15-17] exhibit a faster increase than the three inventories used in our study (see Methods; Extended Data Fig. 4a), which is largely attributed to the interactive effects between climate change and N additions as well as spatio-temporal variability in environmental factors such as rainfall and temperature that modulate the $N_2O$ yield from nitrification and denitrification. This result is in line with the elevated emission factor (EF) deduced from the TD estimates, in which the inversion-based soil emissions increased at a faster rate than suggested by the IPCC Tier 1 EF[14] (which assumes a linear response), especially after 2009 (ref. [18]). The remaining causes of the increase are attributed to other direct anthropogenic sources (6%) and perturbed fluxes from climate/$CO_2$/land cover change (8%). The part of fossil fuel and industry emissions decreased rapidly over 1980–2000 largely due to the installation of emissions abatement equipment in industrial facilities producing nitric and adipic acid. However, after 2000 such emissions began to increase slowly due to rising fossil fuel combustion (Extended Data Fig. 5a-b).

Our analysis of process-based model estimates indicates that soil $N_2O$ emissions accelerated substantially due to climate change since the early 1980s, which has offset the reduction due to elevated $CO_2$ concentration (Extended Data Fig. 6a). Elevated $CO_2$ enhances plant growth and thus increases N uptake, which in turn decreases soil $N_2O$ emissions[16,19]. Land conversion from tropical mature forests with higher $N_2O$ emissions to pastures and other unfertilized agricultural lands has significantly reduced global natural $N_2O$ emissions[11,20,21]. This decrease, however, was

partly offset by an increase in soil $N_2O$ emissions attributable to the temporary rise of emissions following deforestation (post-deforestation pulse effect) and background emissions from converted croplands or pastures[21] (see Methods; Extended Data Fig. 7).

From the ensemble of process-based land model emissions[15,16], we estimate a global agricultural soil EF of 1.8% (1.3%–2.3%), which is significantly larger than the IPCC Tier-1 default for direct emission of 1%. This higher EF, derived from process-based models, suggests a strong interactive effect between N additions and other global environmental changes (Table 1, Perturbed fluxes from climate, atmospheric $CO_2$, and land cover change). Previous field experiments reported a better fit to local observations of soil $N_2O$ emissions when assuming a non-linear response to fertilizer N inputs under varied climate and soil conditions[17,22]. The non-linear response is likely also associated with long-term N accumulation in agricultural soils from N fertilizer use and in aquatic systems from N loads (the legacy effect)[18,23], which provides more substrate for microbial processes[18,24]. The increasing $N_2O$ emissions estimated by process-based models[16] also suggest that recent climate change (particularly warming) may have boosted soil nitrification and denitrification processes, contributing to the growing trend in $N_2O$ emissions together with rising N additions to agricultural soils[16,25-27] (Extended Data Fig. 8).

**Regional $N_2O$ Budgets (2007–2016)**

BU approaches give estimates of $N_2O$ emissions in the five source categories, while TD approaches only provide total emissions (Fig. 2). BU and TD approaches indicate that Africa was the largest $N_2O$ source in the last decade, followed by South America (Fig. 2). BU and TD approaches agree well in the magnitudes and trends of $N_2O$ emissions from South Asia and Oceania (Extended Data Fig. 3j, l). For the remaining regions, BU and TD estimates are

252 comparable in their trends but diverge in their source strengths. Clearly, much more work on
253 regional $N_2O$ budgets is needed, particularly for South America and Africa where we see larger
254 differences between BU and TD estimates and larger uncertainty in each approach. Advancing
255 the understanding and model representation of key processes responsible for $N_2O$ emissions from
256 land and ocean are priorities for reducing uncertainties in BU estimates. Atmospheric
257 observations in underrepresented regions of the world and better atmospheric transport models
258 are essential for uncertainty reduction in TD estimates, while more accurate activity data and
259 robust EFs are critical for GHG inventories (See Methods for additional discussion on
260 uncertainty).

261 Based on the Global $N_2O$ Model Intercomparison Project (NMIP) estimates[16], natural soil
262 emissions (to different extents) dominated in tropical and sub-tropical regions. Soil $N_2O$
263 emissions in the tropics ($0.1\pm0.04$ g N $m^{-2}$ $yr^{-1}$) are about 50% higher than the global average,
264 since many lowland, highly-weathered tropical soils have excess N relative to phosphorus[20].
265 Total anthropogenic emissions in the ten terrestrial regions were highest in East Asia (1.5;
266 0.8−2.6 Tg N $yr^{-1}$), followed by North America, Africa, and Europe. High direct agricultural $N_2O$
267 emissions can be attributed to large-scale synthetic N fertilizer applications in East Asia, Europe,
268 South Asia, and North America, which together consume over 80% of the world's synthetic N
269 fertilizers[28]. In contrast, direct agricultural emissions from Africa and South America are mainly
270 induced by livestock manure that is deposited in pastures and rangelands[28,29]. East Asia
271 contributed 71%−79% of global aquaculture $N_2O$ emissions; South Asia and Southeast Asia
272 together contributed 10%−20% (refs. [30,31]). Indirect emissions play a moderate role in the total
273 $N_2O$ budget, with the highest emission in East Asia (0.3; 0.1−0.5 Tg N $yr^{-1}$). Other direct

anthropogenic sources together contribute $N_2O$ emissions of approximately 0.2−0.4 Tg N $yr^{-1}$ in East Asia, Africa, North America, and Europe.

Both BU and TD estimates of ocean $N_2O$ emissions for northern, tropical, and southern ocean regions (90°−30°N, 30°N−30°S, and 30°−90°S, respectively) reveal that the tropical oceans contribute over 50% to the global oceanic source. In particular, the upwelling regions of the equatorial Pacific, Indian and tropical Atlantic (Fig. 3) provide significant sources of $N_2O$[32-34]. BU estimates suggest the southern ocean is the second largest regional contributor with emissions about twice as high as from the northern oceans (53% tropical oceans, 31% southern oceans, 17% northern oceans), in line with their area, while the TD estimates suggest approximately equal contributions from the southern and northern oceans.

**Four Decades of Anthropogenic $N_2O$ Emissions**

Trends in anthropogenic emissions varied among regions (Fig. 3). Fluxes from Europe and Russia decreased by a total of 0.6 (0.5−0.7) Tg N $yr^{-1}$ over the past 37 years (1980–2016). The decrease in Europe is associated with successful emissions abatement in industry as well as agricultural policies, while the decrease in Russia is associated with the collapse of the agricultural cooperative system after 1990. In contrast, fluxes from the remaining eight regions increased by a total of 2.9 (2.4−3.4) Tg N $yr^{-1}$ (Fig. 3), of which 34% came from East Asia, 18% from Africa, 18% from South Asia, 13% from South America, only 6% from North America, and with remaining increases due to other regions.

The relative importance of each anthropogenic source to the total emission increase differs among regions. East Asia, South Asia, Africa, and South America show larger increases in total agricultural $N_2O$ emissions (direct and indirect) compared to the remaining six regions during

297 1980−2016 (Fig. 3). Southeast Asia, North America, and Middle East also show increasing direct
298 $N_2O$ emissions but to smaller extent. Rising indirect emissions in these four regions (East Asia,
299 South Asia, Africa, and South America) on average constitute 20% of total agricultural $N_2O$
300 emissions and are largely induced by the considerable increase in fertilizer N inputs to
301 agricultural soils[35,36]. The most rapid increase in emissions from other direct anthropogenic
302 sources was found in East Asia, primarily owing to the fast-growing industrial emissions. Africa
303 and South Asia show a fast emission increase due to emissions from fossil fuel and industry and
304 waste and waste water.

305 Our findings point to growing $N_2O$ emissions in emerging economies, particularly Brazil,
306 China, and India. For example, we find here that the substantial increases in livestock manure
307 left on pasture and in fertilizer use caused a ~120% increase in Brazilian agricultural $N_2O$
308 emissions during 1980−2016 (Extended Data Fig. 9). In addition to fertilizer applications, global
309 livestock manure production has been growing steadily, in line with increased livestock
310 numbers[15,28]. Rising demand for meat and dairy products has significantly increased global $N_2O$
311 emissions from livestock manure production and management associated with the expansion of
312 pastures and grazing land[37]. Meanwhile, expansion of feed crop production to support the growth
313 of livestock could further enhance global $N_2O$ emissions[37,38]. Likewise, increasing demand for
314 fish has triggered a five-fold increase in global aquaculture production since the late 1980s[39],
315 with demand projected to increase further[40], although this remains a small fraction (<1%) of total
316 $N_2O$ emissions.

317 The acceleration of global $N_2O$ emissions resulting from anthropogenic sources is apparent in
318 both BU and TD results and currently tracks the highest Representative Concentration Pathway
319 (RCP8.5)[4] in the fifth assessment report (AR5) of IPCC[2] and exceeds all the Shared

Socioeconomic Pathways (SSPs)[3] in CMIP6 for the sixth assessment report (AR6) of IPCC (Fig. 4). Observed atmospheric $N_2O$ concentrations are beginning to exceed predicted levels across all scenarios. Emissions need to be reduced to a level that is consistent with or below that in RCP2.6 or SSP1-2.6 in order to limit warming well below the 2°C target of the Paris Agreement. Failure to include $N_2O$ within climate mitigation strategies will necessitate even greater abatement of $CO_2$ and $CH_4$. Although $N_2O$ mitigation is difficult because N is the key-limiting nutrient in the agricultural production, this study demonstrates that effective mitigation actions have reduced emissions in some regions, such as Europe, through technological improvements in industry and improved N use efficiency in agriculture.

There are a number of mitigation options in the agriculture sector available for immediate deployment, including increased N use efficiency in (i) animal production through tuning of feed rations to reduce N excretion, and (ii) in crop production through precision delivery of N fertilizers, split applications and better timing to match N applications to crop demand, conservation tillage, prevention of waterlogging, and the use of nitrification inhibitors[43,44]. Success stories include the stabilization or reduction of $N_2O$ emissions through improving N use efficiency in the United States and Europe, while maintaining or even increasing crop yields[44,45]. There is every reason to expect that additional implementation of more sustainable practices and emerging technologies will lead to further reductions in these regions. For example, $N_2O$ emissions from European agricultural soils decreased by 21% between 1990 and 2010, a decline attributable to the implementation of the Nitrates Directive (an agricultural policy favoring optimization and reduction of fertilizer use as well as water protection legislation)[46]. For regions where emissions are growing, an immediate opportunity lies in the reduction of excess fertilizer use along with the implementation of more sustainable agricultural practices that together have

been shown to increase crop yields, reduce $N_2O$ emissions, increase water quality, and increase farm income[47]. In addition, $N_2O$ emissions can be efficiently abated in the chemical industry[11,43,48,49], as has been achieved successfully in nitric acid plants in the European Union where industrial $N_2O$ emissions dropped from 11% to 3% of total emissions between 2007 and 2012 (ref. [46]). Additional available strategies to reduce $N_2O$ emissions include promoting lower meat consumption in some parts of the world[9] and reducing food waste[11].

We present the most comprehensive global $N_2O$ budget to date, with a detailed sectorial and regional attribution of sources and sinks. Each of the past four decades had higher global $N_2O$ emissions than the previous one, and in all, agricultural activities dominated the growth in emissions. Total industrial emissions have been quite stable with increased emissions from the fossil fuel sector offset to some extent by the decline in emissions in other industrial sectors as a result of successful abatement policies. We also highlight a number of complex interactions between $N_2O$ fluxes and human-driven changes whose impact on the global atmospheric $N_2O$ growth rate was previously unknown. Those interactions include the effects of climate change, increasing atmospheric $CO_2$, and deforestation. Cumulatively, these exert a relatively small effect on the overall $N_2O$ growth, however, individual flux components, such as the growing positive climate-$N_2O$ feedback, are significant. These fluxes are not currently included in the national GHG reporting. We further find that Brazil, China, and India dominate the regional contributions to the increase in global $N_2O$ emissions over the most recent decade. Our extensive database and modelling capability fill current gaps in national and regional emissions inventories. Future research is needed to further constrain complex biogeochemical interactions between natural/anthropogenic fluxes and global environmental changes, which could lead to significant feedbacks in the future. Reducing excess N applications to croplands and adopting

366 precision fertilizer application methods provide the largest immediate opportunities for $N_2O$

367 emissions abatement.

368

369 **References**


370 1 Prather, M. J. *et al.* Measuring and modeling the lifetime of nitrous oxide including its
371 variability. *Journal of Geophysical Research: Atmospheres* **120**, 5693-5705 (2015).
372 2 Ciais, P. *et al.* in *Climate Change 2013: The Physical Science Basis. Contribution of*
373 *Working Group I to the Fifth Assessment Report of the Intergovernmental Panel on*
374 *Climate Change* 465-570 (Cambridge University Press, 2014).
375 3 Gidden, M. J. *et al.* Global emissions pathways under different socioeconomic scenarios
376 for use in CMIP6: a dataset of harmonized emissions trajectories through the end of the
377 century. *Geoscientific Model Development* **12**, 1443-1475 (2019).
378 4 Davidson, E. A. Representative concentration pathways and mitigation scenarios for
379 nitrous oxide. *Environmental Research Letters* **7**, 024005 (2012).
380 5 Hall, B., Dutton, G. & Elkins, J. The NOAA nitrous oxide standard scale for atmospheric
381 observations. *Journal of Geophysical Research: Atmospheres* **112**, D09305 (2007).
382 6 Prinn, R. G. *et al.* History of chemically and radiatively important atmospheric gases
383 from the Advanced Global Atmospheric Gases Experiment (AGAGE). *Earth System*
384 *Science Data* **10**, 985-1018 (2018).
385 7 Butterbach-Bahl, K., Baggs, E. M., Dannenmann, M., Kiese, R. & Zechmeister-
386 Boltenstern, S. Nitrous oxide emissions from soils: how well do we understand the
387 processes and their controls? *Phil. Trans. R. Soc. B* **368**, 20130122 (2013).
388 8 Tian, H. *et al.* The terrestrial biosphere as a net source of greenhouse gases to the
389 atmosphere. *Nature* **531**, 225-228 (2016).
390 9 UNEP. Drawing down $N_2O$ to protect climate and the ozone layer. Report No.
391 9280733583, (United Nations Environment Programme (UNEP), 2013).
392 10 Park, S. *et al.* Trends and seasonal cycles in the isotopic composition of nitrous oxide
393 since 1940. *Nature Geoscience* **5**, 261-265 (2012).
394 11 Davidson, E. A. & Kanter, D. Inventories and scenarios of nitrous oxide emissions.
395 *Environmental Research Letters* **9**, 105012 (2014).
396 12 Reay, D. S. *et al.* Global agriculture and nitrous oxide emissions. *Nature Climate Change*
397 **2**, 410-416 (2012).
398 13 Syakila, A. & Kroeze, C. The global nitrous oxide budget revisited. *Greenhouse Gas*
399 *Measurement and Management* **1**, 17-26 (2011).
400 14 IPCC. 2006 IPCC Guidelines for National Greenhouse Gas Inventories., (Japan on behalf
401 of the IPCC, Hayama, Japan, 2006).
402 15 Dangal, S. R. *et al.* Global nitrous oxide emissions from pasturelands and rangelands:
403 Magnitude, spatio-temporal patterns and attribution. *Global Biogeochemical Cycles* **33**,
404 200-222 (2019).
405 16 Tian, H. Q. *et al.* Global soil nitrous oxide emissions since the preindustrial era estimated
406 by an ensemble of terrestrial biosphere models: Magnitude, attribution, and uncertainty.
407 *Global Change Biology* **25**, 640-659 (2019).

17 Wang, Q. *et al.* Data-driven estimates of global nitrous oxide emissions from croplands. *National Science Review* **7**, 441-452 (2020).
18 Thompson, R. L. *et al.* Acceleration of global $N_2O$ emissions seen from two decades of atmospheric inversion. *Natural Climate Change* **9**, 993-998 (2019).
19 Zaehle, S., Ciais, P., Friend, A. D. & Prieur, V. Carbon benefits of anthropogenic reactive nitrogen offset by nitrous oxide emissions. *Nature Geoscience* **4**, 601-605 (2011).
20 Davidson, E. A. *et al.* Recuperation of nitrogen cycling in Amazonian forests following agricultural abandonment. *Nature* **447**, 995-998 (2007).
21 Verchot, L. V. *et al.* Land use change and biogeochemical controls of nitrogen oxide emissions from soils in eastern Amazonia. *Global Biogeochemical Cycles* **13**, 31-46 (1999).
22 Shcherbak, I., Millar, N. & Robertson, G. P. Global metaanalysis of the nonlinear response of soil nitrous oxide ($N_2O$) emissions to fertilizer nitrogen. *Proceedings of the National Academy of Sciences* **111**, 9199-9204 (2014).
23 Van Meter, K. J., Basu, N. B., Veenstra, J. J. & Burras, C. L. The nitrogen legacy: emerging evidence of nitrogen accumulation in anthropogenic landscapes. *Environmental Research Letters* **11**, 035014 (2016).
24 Firestone, M. K. & Davidson, E. A. Microbiological basis of NO and $N_2O$ production and consumption in soil. *Exchange of trace gases between terrestrial ecosystems the atmosphere* **47**, 7-21 (1989).
25 Griffis, T. J. *et al.* Nitrous oxide emissions are enhanced in a warmer and wetter world. *Proceedings of the National Academy of Sciences* **114**, 12081-12085 (2017).
26 Pärn, J. *et al.* Nitrogen-rich organic soils under warm well-drained conditions are global nitrous oxide emission hotspots. *Nature Communications* **9**, 1135 (2018).
27 Smith, K. The potential for feedback effects induced by global warming on emissions of nitrous oxide by soils. *Global Change Biology* **3**, 327-338 (1997).
28 FAOSTAT. The Food and Agriculture Organization of the United Nations Statistics: Emissions-Agriculture, Emissions Land Use Trade (Crops and livestock products), Population, Agri-Environmental Indicators (Livestock Manure) (2019).
29 Xu, R. *et al.* Increased nitrogen enrichment and shifted patterns in the world's grassland: 1860–2016. *Earth System Science Data* **11**, 175-187 (2019).
30 Beusen, A. H., Bouwman, A. F., Van Beek, L. P., Mogollón, J. M. & Middelburg, J. J. Global riverine N and P transport to ocean increased during the 20th century despite increased retention along the aquatic continuum. *Biogeosciences* **13**, 2441-2451 (2016).
31 MacLeod, M., Hasan, M. R., Robb, D. H. F. & Mamun-Ur-Rashid, M. Quantifying and mitigating greenhouse gas emissions from global aquaculture. *FAO, Rome* (2019).
32 Buitenhuis, E. T., Suntharalingam, P. & Le Quéré, C. Constraints on global oceanic emissions of $N_2O$ from observations and models. *Biogeosciences* **15**, 2161-2175 (2018).
33 Manizza, M., Keeling, R. F. & Nevison, C. D. On the processes controlling the seasonal cycles of the air–sea fluxes of $O_2$ and $N_2O$: A modelling study. *Tellus B: Chemical and Physical Meteorology* **64**, 18429 (2012).
34 Martinez-Rey, J., Bopp, L., Gehlen, M., Tagliabue, A. & Gruber, N. Projections of oceanic $N_2O$ emissions in the 21st century using the IPSL Earth system model. *Biogeosciences* **12**, 4133-4148 (2015).
35 Maavara, T. *et al.* Nitrous oxide emissions from inland waters: Are IPCC estimates too high? *Global Change Biology* **25**, 473-488 (2019).

36 Yao, Y. *et al.* Increased global nitrous oxide emissions from streams and rivers in the Anthropocene. *Natural Climate Change* **10**, 138-142 (2020).
37 Gerber, P. J. *et al. Tackling climate change through livestock: a global assessment of emissions and mitigation opportunities*. *FAO* (2013).
38 Herrero, M. *et al.* Biomass use, production, feed efficiencies, and greenhouse gas emissions from global livestock systems. *Proceedings of the National Academy of Sciences* **110**, 20888-20893 (2013).
39 Yuan, J. *et al.* Rapid growth in greenhouse gas emissions from the adoption of industrial-scale aquaculture. *Nature Climate Change* **9**, 318-322 (2019).
40 Froehlich, H. E., Runge, C. A., Gentry, R. R., Gaines, S. D. & Halpern, B. S. Comparative terrestrial feed and land use of an aquaculture-dominant world. *Proceedings of the National Academy of Sciences* **115**, 5295-5300 (2018).
41 O'Neill, B. C. *et al.* The Scenario Model Intercomparison Project (ScenarioMIP) for CMIP6. *Geoscience Model Development* **9**, 3461-3482 (2016).
42 Gütschow, J. *et al.* The PRIMAP-hist national historical emissions time series. *Earth System Science Data* **8**, 571-603 (2016).
43 Winiwarter, W., Höglund-Isaksson, L., Klimont, Z., Schöpp, W. & Amann, M. Technical opportunities to reduce global anthropogenic emissions of nitrous oxide. *Environmental Research Letters* **13**, 014011 (2018).
44 Zhang, X. *et al.* Managing nitrogen for sustainable development. *Nature* **528**, 51-59 (2015).
45 Mueller, N. D. *et al.* Declining spatial efficiency of global cropland nitrogen allocation. *Global Biogeochemical Cycles* **31**, 245-257 (2017).
46 European Environment Agency. Annual European Union greenhouse gas inventory 1990-2017 and inventory report 2019. *Submission under the United Nations Framework Convention on Climate Change and the Kyoto Protocol, Copenhagen, DK* (2019).
47 Cui, Z. *et al.* Pursuing sustainable productivity with millions of smallholder farmers. *Nature* **555**, 363-366 (2018).
48 Kanter, D. *et al.* A post-Kyoto partner: considering the stratospheric ozone regime as a tool to manage nitrous oxide. *Proceedings of the National Academy of Sciences* **110**, 4451-4457 (2013).
49 Schneider, L., Lazarus, M. & Kollmuss, A. J. S. M. S. E. I. Industrial $N_2O$ projects under the CDM: Adipic acid-A case of carbon leakage. *Stockholm Environment Institute* (2010).

**Table 1 The global $N_2O$ budget in the 1980s, 1990s, 2000s, and 2007–2016.**

| | | the 1980s | | | the 1990s | | | the 2000s | | | 2007-2016 | | |
|---|---|---|---|---|---|---|---|---|---|---|---|---|---|
| ***Anthropogenic sources*** | | **mean** | **min** | **max** | **mean** | **min** | **max** | **mean** | **min** | **max** | **mean** | **min** | **max** |
| Direct emissions of N additions in the agricultural sector (Agriculture) | Direct soil emissions | 1.5 | 0.9 | 2.6 | 1.7 | 1.1 | 3.1 | 2.0 | 1.3 | 3.4 | 2.3 | 1.4 | 3.8 |
| | Manure left on pasture | 0.9 | 0.7 | 1.0 | 1.0 | 0.7 | 1.1 | 1.1 | 0.8 | 1.2 | 1.2 | 0.9 | 1.3 |
| | Manure management | 0.3 | 0.2 | 0.4 | 0.3 | 0.2 | 0.4 | 0.3 | 0.2 | 0.5 | 0.3 | 0.2 | 0.5 |
| | Aquaculture | 0.01 | 0.00 | 0.03 | 0.03 | 0.01 | 0.1 | 0.1 | 0.02 | 0.2 | 0.1 | 0.02 | 0.2 |
| | sub-total | 2.6 | 1.8 | 4.1 | 3.0 | 2.1 | 4.8 | 3.4 | 2.3 | 5.2 | 3.8 | 2.5 | 5.8 |
| Other direct anthropogenic sources | Fossil fuel and industry | 0.9 | 0.8 | 1.1 | 0.9 | 0.9 | 1.0 | 0.9 | 0.8 | 1.0 | 1.0 | 0.8 | 1.1 |
| | Waste and waste water | 0.2 | 0.1 | 0.3 | 0.3 | 0.2 | 0.4 | 0.3 | 0.2 | 0.4 | 0.3 | 0.2 | 0.5 |
| | Biomass burning | 0.7 | 0.7 | 0.7 | 0.7 | 0.6 | 0.8 | 0.6 | 0.6 | 0.6 | 0.6 | 0.5 | 0.8 |
| | sub-total | 1.8 | 1.6 | 2.1 | 1.9 | 1.7 | 2.1 | 1.8 | 1.6 | 2.1 | 1.9 | 1.6 | 2.3 |
| Indirect emissions from anthropogenic N additions | Inland waters, estuaries, coastal zones | 0.4 | 0.2 | 0.5 | 0.4 | 0.2 | 0.5 | 0.4 | 0.2 | 0.6 | 0.5 | 0.2 | 0.7 |
| | Atmospheric N deposition on land | 0.6 | 0.3 | 1.2 | 0.7 | 0.4 | 1.4 | 0.7 | 0.4 | 1.3 | 0.8 | 0.4 | 1.4 |
| | Atmospheric N deposition on ocean | 0.1 | 0.1 | 0.2 | 0.1 | 0.1 | 0.2 | 0.1 | 0.1 | 0.2 | 0.1 | 0.1 | 0.2 |
| | sub-total | 1.1 | 0.6 | 1.9 | 1.2 | 0.7 | 2.1 | 1.2 | 0.6 | 2.1 | 1.3 | 0.7 | 2.2 |
| Perturbed fluxes from climate/$CO_2$/land cover change | $CO_2$ effect | -0.2 | -0.3 | 0.0 | -0.2 | -0.4 | 0.0 | -0.3 | -0.5 | 0.1 | -0.3 | -0.6 | 0.1 |
| | Climate effect | 0.4 | 0.0 | 0.8 | 0.5 | 0.1 | 0.9 | 0.7 | 0.3 | 1.2 | 0.8 | 0.3 | 1.3 |
| | Post-deforestation pulse effect | 0.7 | 0.6 | 0.8 | 0.7 | 0.6 | 0.8 | 0.7 | 0.7 | 0.8 | 0.8 | 0.7 | 0.8 |
| | Long-term effect of reduced mature forest area | -0.8 | -0.8 | -0.9 | -0.9 | -0.8 | -1.0 | -1.0 | -0.9 | -1.1 | -1.1 | -1.0 | -1.1 |
| | sub-total | 0.1 | -0.4 | 0.7 | 0.1 | -0.5 | 0.7 | 0.2 | -0.4 | 0.9 | 0.2 | -0.6 | 1.1 |
| Anthropogenic total | | 5.6 | 3.6 | 8.7 | 6.2 | 3.9 | 9.7 | 6.7 | 4.1 | 10.3 | 7.3 | 4.2 | 11.4 |
| ***Natural fluxes*** | | | | | | | | | | | | | |
| Natural soils baseline | | 5.6 | 4.9 | 6.6 | 5.6 | 4.9 | 6.5 | 5.6 | 5.0 | 6.5 | 5.6 | 4.9 | 6.5 |
| Ocean baseline | | 3.6 | 3.0 | 4.4 | 3.5 | 2.8 | 4.4 | 3.5 | 2.7 | 4.3 | 3.4 | 2.5 | 4.3 |
| Natural (Inland waters, estuaries, coastal zones) | | 0.3 | 0.3 | 0.4 | 0.3 | 0.3 | 0.4 | 0.3 | 0.3 | 0.4 | 0.3 | 0.3 | 0.4 |
| Lightning and atmospheric production | | 0.4 | 0.2 | 1.2 | 0.4 | 0.2 | 1.2 | 0.4 | 0.2 | 1.2 | 0.4 | 0.2 | 1.2 |
| Surface sink | | -0.01 | 0.00 | -0.3 | -0.01 | 0.00 | -0.3 | -0.01 | 0.00 | -0.3 | -0.01 | 0.00 | -0.3 |
| Natural total | | 9.9 | 8.5 | 12.2 | 9.8 | 8.3 | 12.1 | 9.8 | 8.2 | 12.0 | 9.7 | 8.0 | 12.0 |
| *Bottom-up total source* | | 15.5 | 12.1 | 20.9 | 15.9 | 12.2 | 21.7 | 16.4 | 12.3 | 22.4 | 17.0 | 12.2 | 23.5 |
| *Top-down Ocean* | | | | | | | | 5.1 | 3.1 | 7.2 | 5.1 | 3.4 | 7.1 |
| *Top-down Land* | | | | | | | | 10.8 | 9.3 | 12.5 | 11.8 | 10.6 | 13.8 |
| *Top-down total source* | | | | | | | | 15.9 | 15.1 | 16.9 | 16.9 | 15.9 | 17.7 |
| *Top-down Statospheric sink* | | | | | | | | 12.1 | 11.4 | 13.1 | 12.4 | 11.7 | 13.3 |
| Observed atmospheric chemical sink* | | | | | | | | 13.3 | 12.2 | 14.4 | 13.5 | 12.4 | 14.6 |
| **Change in atmospheric abundance**** | | | | | | | | **3.7** | **3.2** | **4.2** | **4.3** | **3.8** | **4.8** |
| Atmospheric burden | | 1462 | 1442 | 1482 | 1493 | 1472 | 1514 | 1531 | 1510 | 1552 | 1555 | 1533 | 1577 |

Note: *BU estimates include four categories of anthropogenic sources (red for agriculture, orange for other direct anthropogenic sources, maroon for indirect emissions from anthropogenic N additions, and brown for perturbed fluxes from climate/$CO_2$/land cover change) and one category for natural sources and sinks (green). The sources and sinks of $N_2O$ are given in Tg N $yr^{-1}$. The atmospheric burden is given in Tg N. *calculated from satellite observations with a photolysis model (about 1% of this sink occurs in the troposphere). **Calculated from the combined NOAA and AGAGE record of surface $N_2O$, and adopting the uncertainty of the IPCC AR5 (Chapter 6)[2]. Detailed information on calculating each sub-category is shown in Supplementary Tables 1–13.*

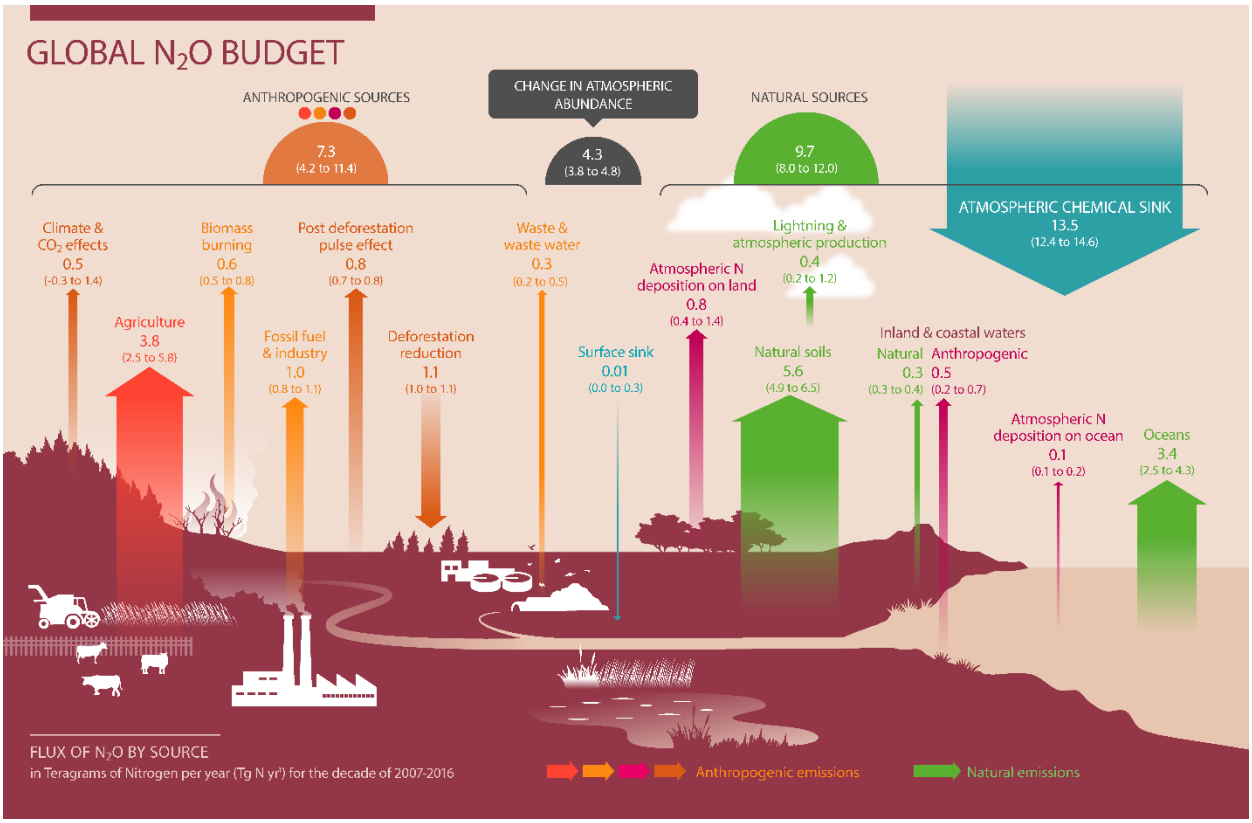


**Fig. 1 Global $N_2O$ budget for the recent decade (2007–2016).** *The red arrow represents direct emissions of N additions in the agricultural sector (Agriculture). The orange arrows represent emissions from other direct anthropogenic sources. The maroon arrows represent indirect emissions from anthropogenic N additions. The brown arrows represent perturbed fluxes from climate/$CO_2$/land cover change effects. The green arrows represent natural source. The anthropogenic and natural $N_2O$ sources are derived from BU estimates. The blue arrows represent surface sink and observed atmospheric chemical sink of which about 1% occurs in the troposphere. The total budget (sources + sinks) does not exactly match the observed atmospheric accumulation, because each of the terms has been derived independently and we do not force top-down agreement by rescaling the terms. This imbalance readily falls within the overall uncertainty in closing the $N_2O$ budget, as reflected in each of the terms. The $N_2O$ sources and sinks are given in Tg N $yr^{-1}$.*

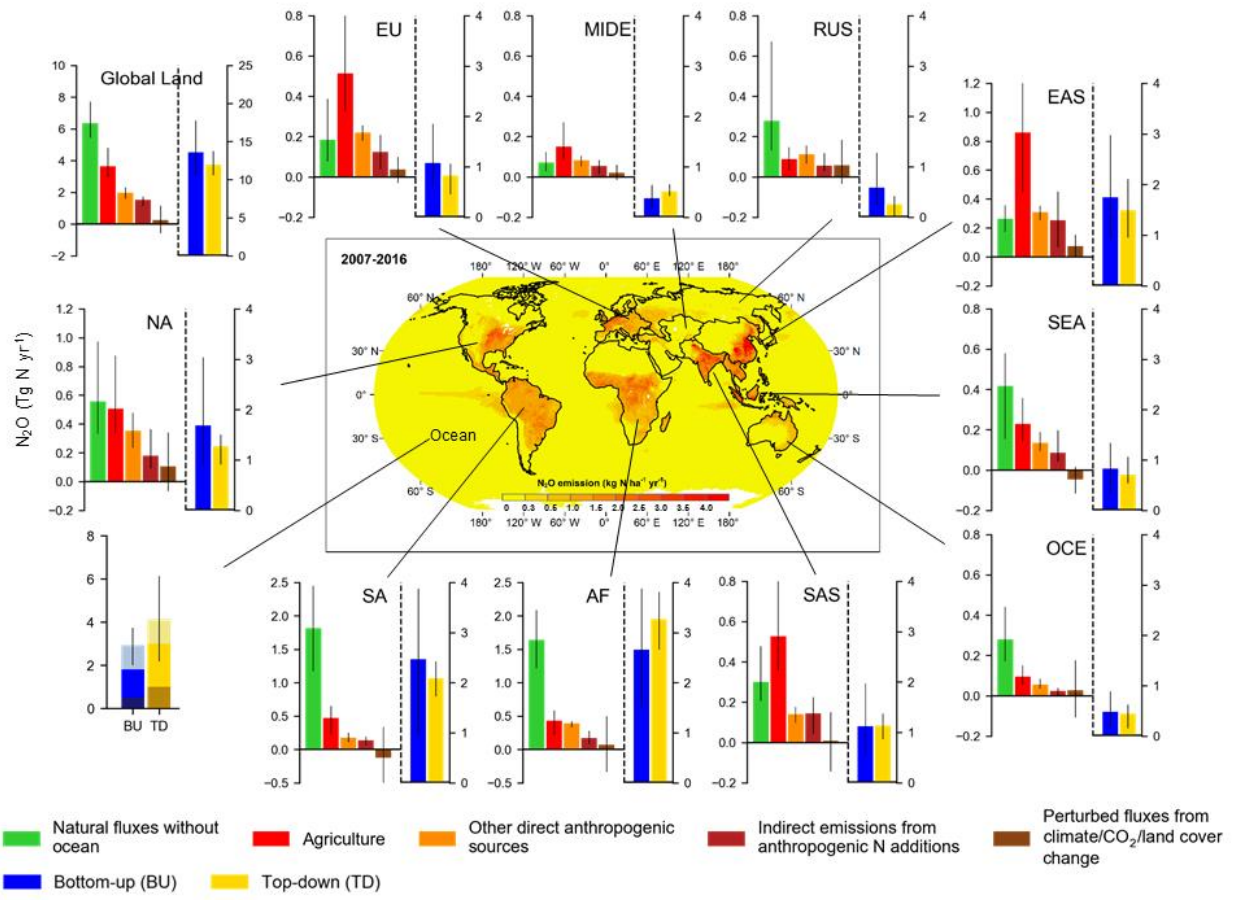


**Fig. 2 Regional $N_2O$ sources in the recent decade (2007–2016) over 11 regions.** *The Earth's ice-free land is partitioned into ten regions: North America (NA), South America (SA), Europe (EU), Middle East (MIDE), Africa (AF), Russia (RUS), East Asia (EAS), South Asia (SAS), Southeast Asia (SEA), and Oceania (OCE). In each subplot from left to right: emissions from five sub-sectors using BU approaches: natural fluxes without ocean (green), direct emissions of N additions in the agricultural sector (Agriculture, red), other direct anthropogenic sources (orange), indirect emissions from anthropogenic N additions (maroon), and perturbed fluxes from climate/$CO_2$/land cover change (brown); the sum of these five categories by BU approaches (blue), and the estimates by TD approaches (gold). BU and TD estimates of ocean emissions are shown at the bottom left (from bottom to top: 30°–90°N, 30°S–30°N, and 90°–30°S). Error bars indicate the spread between the minimum and the maximum values. The center map shows the spatial distribution of 10-year average $N_2O$ emissions from land and ocean based on the land and ocean models. Per capita $N_2O$ emission (kg N capita$^{-1}$ yr$^{-1}$) during 2007–2016 is shown in Supplementary Fig. 2.*

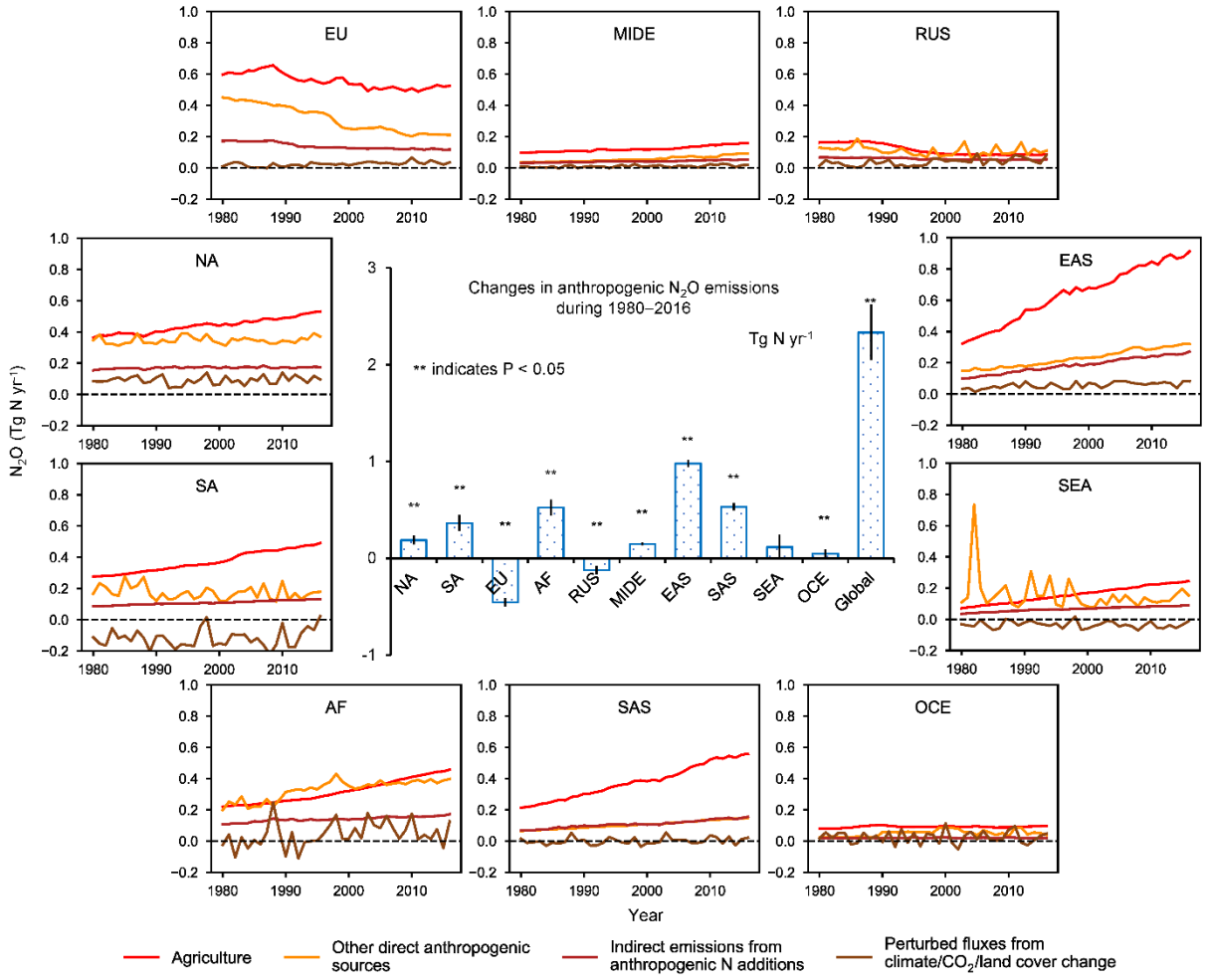


**Fig. 3 Ensembles of regional anthropogenic $N_2O$ emissions over the 1980–2016 period.** *The bar chart in the center shows the accumulated changes in regional and global $N_2O$ emissions during the study period. Error bars indicate the 95% confidence interval for the average of accumulated changes. The Mann-Kendall test was performed to examine a monotonic increasing or decreasing trend in the estimated ensemble $N_2O$ emissions for each region and the globe during 1980–2016. The accumulated changes were calculated from the linear regressed annual change rate (Tg N $yr^{-2}$) multiplied by 37 years. All regions except SEA show a significant increasing or decreasing trend in the estimated ensemble $N_2O$ emissions during the study period (indicated by ** for each bar).*

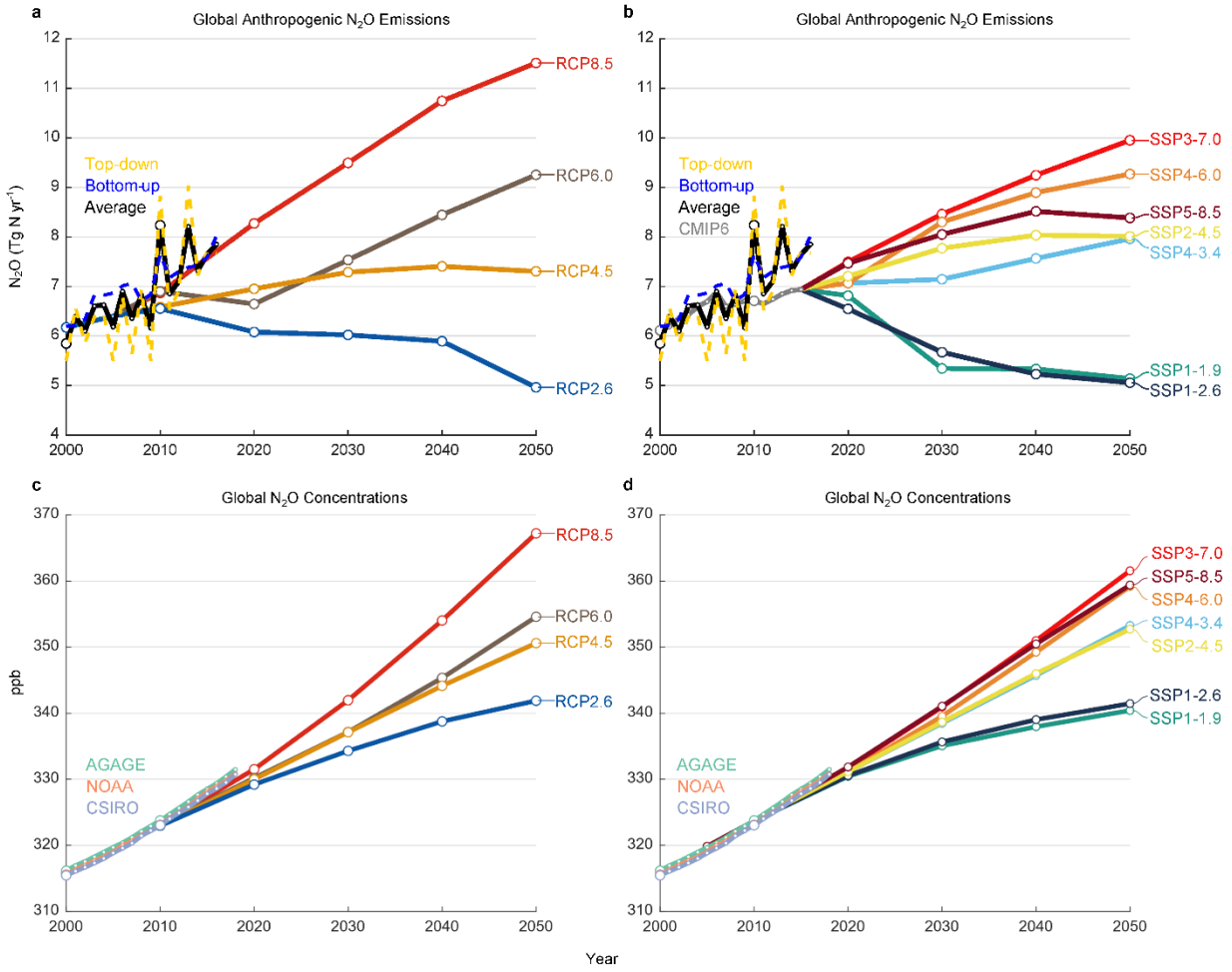


**Fig. 4 Historical and projected global anthropogenic $N_2O$ emissions and concentrations.** *Global anthropogenic $N_2O$ emissions (**a, b**) and concentrations (**c, d**) compared to the four representative concentration pathways (RCPs) in the IPCC AR5 (**a**, **c**, ref. [2]) and the new marker scenarios based on the Shared Socioeconomic Pathways (SSPs) used in CMIP6 (**b**, **d**, ref. [41]). The historical data is represented as the mean of the BU and TD estimates of anthropogenic $N_2O$ emissions, while the atmospheric concentration uses the three observation networks available, AGAGE, NOAA, and CSIRO. TD anthropogenic emissions were calculated by subtracting BU-derived natural fluxes. To aid the comparison, the four RCPs were shifted down so that the 2005 value is equal to the 2000–2009 average of the mean of TD and BU estimates. The SSPs are harmonized[3] to match the historical emissions used in CMIP6[42] and Extended Data Fig. 10 shows the unharmonized data.*

## Methods

**Terminology.** This study provides an estimation of the global $N_2O$ budget considering all possible sources and all global change processes that can perturb the budget. A total of 18 sources and three sinks of $N_2O$ are identified and grouped into six categories (Figure 1, Table 1): 1) Natural fluxes in absence of climate change and anthropogenic disturbances including Soil emissions, Surface sink, Ocean emissions, Lightning and atmospheric production, and Natural emission from inland waters, estuaries, coastal zones (inland and coastal waters), 2) Perturbed fluxes from climate/$CO_2$/land cover change including $CO_2$ effect, Climate effect, Post-deforestation pulse effect, and Long-term effect of reduced mature forest area, 3) Direct emissions of N additions in the agricultural sector (Agriculture) including emissions from direct application of synthetic N fertilizers and manure (henceforth Direct soil emissions), Manure left on pasture, Manure management, and Aquaculture, 4) Indirect emissions from anthropogenic N additions including atmospheric N deposition (NDEP) on land, atmospheric NDEP on ocean, and effects of anthropogenic loads of reactive N in inland waters, estuaries, coastal zones, 5) Other direct anthropogenic sources including Fossil fuel and industry, Waste and waste water, and Biomass burning, and 6) Two estimates of stratospheric sinks obtained from atmospheric chemistry transport models and observations, and one tropospheric sink (Table 1, Extended Data Fig. 2).

For the purpose of compiling national GHG inventories for country reporting to the climate convention, our anthropogenic $N_2O$ emission categories are aligned with those used in UNFCCC reporting and IPCC 2006 methodologies (Supplementary Table 14). We also provide the detailed comparison of our methodology and quantification with the IPCC AR5 (see Supplementary Section 4; Supplementary Table 15).

583 **Data synthesis.** We consider global $N_2O$ emission from land and ocean consisting of natural
584 fluxes and anthropogenic emissions based on BU and TD approaches, however, the TD approach
585 cannot separate natural and anthropogenic sources.

586 'Natural soil baseline' emissions were obtained from six terrestrial biosphere models
587 (NMIP[16], Supplementary Tables 16–17) and provided here reflect a situation without
588 consideration of land use change (e.g., deforestation) and without consideration of indirect
589 anthropogenic effects via global change (i.e., climate, elevated $CO_2$, and atmospheric N
590 deposition). BU oceanic $N_2O$ emissions were based on an inter-comparison of five global ocean
591 biogeochemistry models (Supplementary Table 18). The natural emission from 'Inland water,
592 estuaries, coastal zones' includes coastal upwelling[50] and inland and coastal waters that were
593 obtained from Yao et al.[36], Maavara et al.[35], and Lauerwald et al.[51]. Since the data (rivers,
594 reservoirs, and estuaries) provided by Maavara et al. and Lauerwald et al. are for the year 2000,
595 we assume that these values are constant during 1980–2016. Yao et al.[36] provided annual
596 riverine $N_2O$ emissions using DLEM during the same period. Here, we averaged estimates from
597 Yao et al. with that from Maavara et al.[35]. In addition, we estimated $N_2O$ emissions from global
598 and regional reservoirs in the 2000s, and averaged their estimates with that from Maavara et al.[35]
599 to represent emissions from reservoirs during 1980–2016. The estimate for global and regional
600 estuaries and lakes is still based on the long-term averaged values provided by Maavara et al.[35]
601 and Lauerwald et al.[51], respectively. We considered the riverine emissions in the year 1900 as
602 equivalent to the natural emission for the DLEM estimate assuming that the N load from land
603 was negligible in that period[52]. We quantified the contribution of natural sources to total
604 emission from reservoirs, lakes, and estuaries at 44% (36%–52%), with consideration of all N
605 inputs (i.e., inorganic, organic, dissolved, particulate forms). We combined the estimate from

606 lightning with that from atmospheric production into an integrated category 'Lightning and
607 atmospheric production'. We make the simplification of considering the category 'Lightning and
608 atmospheric production' as purely natural, however, atmospheric production is affected to some
609 extent by anthropogenic activities through enhancing the concentrations of the reactive species
610 $NH_2$ and $NO_2$. This category is in any case very small and the anthropogenic enhancement effect
611 is uncertain. Lightning produces $NO_x$, the median estimate of which is 5 Tg N $yr^{-1}$ (ref. [53]). We
612 assumed an EF of 1% (ref. [54]) and a global estimate of 0.05 (0.02–0.09) Tg N $yr^{-1}$ from lightning.
613 Atmospheric production of $N_2O$ results from the reaction of $NH_2$ with $NO_2$ (refs. [55,56]), N with
614 $NO_2$, and oxidation of $N_2$ by $O(^1D)$[57], all of which constitute an estimated source of 0.3 (0.2–1.1)
615 Tg N $yr^{-1}$. The estimate of 'Surface sink' was obtained from Schlesinger[58] and Syakila et al.[59].
616 The anthropogenic sources include four sub-sectors:
617 **(a) Agriculture.** It consists of four components: 'Direct soil emissions', 'Manure left on
618 pasture', 'Manure management', and 'Aquaculture'. Data for 'Direct soil emissions' were
619 obtained as the ensemble mean of $N_2O$ emissions from an average of three inventories (EDGAR
620 v4.3.2, FAOSTAT, and GAINS), the SRNM/DLEM models, and the NMIP/DLEM models. The
621 statistical model SRNM only covers cropland $N_2O$ emissions, the same as the NMIP. Thus, we
622 add the DLEM-based estimate of pasture $N_2O$ emissions into the two estimates in cropland to
623 represent direct agricultural soil emissions (i.e., SRNM/DLEM or NMIP/DLEM). The 'Manure
624 left on pasture' and 'Manure management' emissions are the ensemble mean of EDGAR v4.3.2,
625 FAOSTAT, and GAINS databases. Global N flows (i.e., fish feed intake, fish harvest, and waste)
626 in freshwater and marine aquaculture were obtained from Beusen et al.[30] and Bouwman et al.[60,61]
627 based on a nutrient budget model for the period 1980–2016. We then calculated global
628 aquaculture $N_2O$ emissions through considering 1.8% loss of N waste in aquaculture, the same

629 EF used in Hu et al.[62] and Macleod et al.[31]. The uncertainty range of the EF is from 0.5% (ref. [14])
630 to 5% (ref. [63]), the same range used in the UNEP report[9]. The 'Aquaculture' emission for the
631 period 2007–2016 was a synthesis data from Hu et al.[62] in 2009, the FAO Report[31] in 2013, and
632 our calculations. The estimate of aquaculture $N_2O$ emission prior to 2009 was from our
633 calculations only.

634 The estimated direct emissions from agriculture have increased from 2.6 (1.8−4.1) Tg N $yr^{-1}$
635 in the 1980s to 3.8 (2.5−5.8) Tg N $yr^{-1}$ over the recent decade (2007–2016, Table 1).
636 Specifically, direct soil emission from the application of fertilizers is the major source and
637 increased at a rate of 0.27±0.01 Tg N $yr^{-1}$ per decade ($P < 0.05$; Table 1). Compared with the
638 three global inventories (FAOSTAT, EDGAR v4.3.2, and GAINS), the estimates from process-
639 based models (NMIP/DLEM[15,16]) and a statistical model (SRNM)/DLEM[15,17] exhibited a faster
640 increase (Extended Data Fig. 4a). Over the past four decades, we also found a small but
641 significant increase in emissions from livestock manure (i.e., manure left on pasture and manure
642 management) at a rate of 0.1±0.01 Tg N $yr^{-1}$ per decade ($P < 0.05$; Extended Data Fig. 4b-c).
643 Meanwhile, global aquaculture $N_2O$ emissions increased 10-fold, however, this flux remains the
644 smallest term in the global budget (Extended Data Fig. 4d).

645 **(b) Other direct anthropogenic sources.** It includes 'Fossil fuel and industry', 'Waste and
646 waste water', and 'Biomass burning'. Both 'Fossil fuel and industry' and 'Waste and waste
647 water' are the ensemble means of EDGAR v4.3.2 and GAINS databases. The 'Biomass burning'
648 emission is the ensemble mean of FAOSTAT, DLEM, and GFED4s databases.

649 Emissions from a combination of fossil fuel and industry, waste and waste water, and biomass
650 burning increased from 1.8 (1.6−2.1) Tg N $yr^{-1}$ in the 1980s to 1.9 (1.6−2.3) Tg N $yr^{-1}$ over the
651 period of 2007–2016 (Table 1). The waste and waste water emission showed a continuous

increase at a rate of 0.04±0.01 Tg N $yr^{-1}$ per decade ($P < 0.05$) (Extended Data Fig. 5c). Emissions from biomass burning, estimated based on three data sources (DLEM, GFED4s, and FAOSTAT), slightly decreased at a rate of -0.03±0.04 Tg N $yr^{-1}$ per decade ($P = 0.3$) since the1980s (Extended Data Fig. 5d). This item is largely affected by climate and land use change[64,65]. Of the three data sources, the DLEM estimate exhibited significant inter-annual variability, especially during 1980–2000 when extreme fire events were detected in 1982, 1987, 1991, 1994, and 1998. The occurrences of these extreme fires were associated with El Niño-Southern Oscillation (ENSO) events, especially in Indonesia (e.g., 'Great Fire of Borneo' in 1982) [66]. Since 1997, $N_2O$ emissions from fires estimated by DLEM, GFED4s, and FAOSTAT were consistent in the inter-annual variability. All the three estimates showed a decreasing trend, agreeing well with satellite-observed decrease of global burned area[64,65].

**(c) Indirect emissions from anthropogenic N additions.** Data were obtained from various sources and considered N deposition on land and ocean ('N deposition on land' and 'N deposition on ocean'), as well as the N leaching and runoff from upstream ('Inland and coastal waters'). The emission from 'N deposition on ocean' was provided by Suntharalingam et al.[67], while emission from 'N deposition on land' was the ensemble mean of an average of three inventories: FAOSTAT/EDGAR v4.3.2, GAINS/EDGAR v4.3.2, and NMIP. FAOSTAT and GAINS documented the sector 'Indirect agricultural $N_2O$ emissions' by separating estimates from N leaching or N deposition, while EDGAR v4.3.2 did not. Here, we treated 'Indirect agricultural $N_2O$ emissions' from EDGAR v4.3.2 as 'Inland and coastal waters' emissions for data synthesis. Only EDGAR v4.3.2 provided an estimate of indirect emission from non-agricultural sectors, while both FAOSTAT and GAINS, following the IPCC guidelines, provided $NH_x/NO_y$ volatilization from agricultural sectors. Here, we sum FAOSTAT or GAINS with

675 EDGAR v4.3.2 (i.e., FAOSTAT/EDGAR v4.3.2 or GAINS/EDGAR v4.3.2) to represent N
676 deposition induced soil emissions from both agricultural and non-agricultural sectors. The $N_2O$
677 emissions from 'Inland and coastal waters' consist of rivers, reservoirs, lakes, estuaries, and
678 coastal zone, which is the ensemble mean of an average of three inventories (EDGAR v4.3.2,
679 FAOSTAT, GAINS), and the mean of process-based models. The anthropogenic emission
680 estimated by Yao et al.[36] considered annual N inputs and other environmental factors (i.e.,
681 climate, elevated $CO_2$, and land cover change). For long-term average in rivers, reservoirs,
682 estuaries and lakes, we applied a mean of 56% (based on the ratio of anthropogenic to total N
683 additions from land) to calculate anthropogenic emissions. Seagrass, mangrove, saltmarsh and
684 intertidal $N_2O$ emissions were undated from Murray et al[68]. Coastal waters with low disturbance
685 generally either have low $N_2O$ emissions or act as a sink for $N_2O$[69,70]. Here, coastal zone
686 emissions were treated as anthropogenic emissions due to intensive human disturbances[71].
687 $N_2O$ emissions following transport of anthropogenic N additions via atmosphere and water
688 bodies increased from 1.1 (0.6−1.9) Tg N $yr^{-1}$ in the 1980s to 1.3 (0.7−2.2) Tg N $yr^{-1}$ during
689 2007−2016 (Table 1). The $N_2O$ emissions from inland and coastal waters increased at a rate of
690 0.03±0.00 Tg N $yr^{-1}$ per decade ($P < 0.05$). Such an increase was reported by all the three
691 inventories (FAOSTAT, GAINS, and EDGAR v4.3.2) with FAOSTAT giving the largest
692 estimate. In contrast, the DLEM-based estimate presented a divergent trend: first increasing from
693 1980−1998 and then slightly decreasing thereafter (Extended Data Fig. 6a). Emissions from
694 atmospheric N deposition on oceans were relatively constant with a value of 0.1 (0.1−0.2) Tg N
695 $yr^{-1}$, while a large increase in emissions was found from atmospheric N deposition on land, with
696 0.06±0.01 Tg N $yr^{-1}$ per decade ($P < 0.05$) reported in the three estimates (FAOSTAT/EDGAR
697 v4.3.2, GAINS/EDGAR v4.3.2, and NMIP). The FAOSTAT agricultural source, together with

the EDGAR v4.3.2 industrial source, is consistent with NMIP estimates in the magnitude of $N_2O$ emissions, with the latter estimating a slightly slower increase from 2010 to 2016 (Extended Data Fig. 6b).

**(d) Perturbed fluxes from climate/$CO_2$/land cover change.** Perturbed $N_2O$ fluxes represent the sum of the effects of climate, elevated atmospheric $CO_2$, and land cover change. The estimate of climate and $CO_2$ effects on emissions was based on NMIP. The effect of land cover change on $N_2O$ dynamics includes the reduction due to 'Long-term effect of reduced mature forest area' and the emissions due to 'Post-deforestation pulse effect'. The two estimates were based on the book-keeping approach and the DLEM model simulation. The book-keeping method is developed by Houghton et al.[72] for accounting for carbon flows due to land use. In this study, an observation dataset consisting of 18 tropical sites was collected to follow the book-keeping logic. The dataset covers $N_2O$ emissions from a reference mature forest and their nearby converted pastures aged between one and 60 years. The average tropical forest $N_2O$ emission rate of 1.974 kg $N_2O$-N $ha^{-1}$ $yr^{-1}$ was adopted as the baseline[73]. Two logarithmic response curves of soil $N_2O$ emissions (normalized to the baseline) after deforestation were developed: $y = -0.31\,ln(x) + 1.53$ ($R^2 = 0.30$) and $y = -0.454\,ln(x) + 2.21$ ($R^2 = 0.09$). The first logarithmic function uses data collected by a review analysis[74], based upon which the second one further considers observations from Verchot et al.[21] and Keller and Reiners[75]. In the first function, *x* (unit: year) indicates pasture age in years after deforestation and *y* (unitless; 0–1) indicates the ratio of pasture $N_2O$ emission over the $N_2O$ emission from the nearby reference mature forest. In the second function, *x* (unit: year) indicates secondary forest age and *y* (unitless; 0–1) indicates the ratio of secondary forest $N_2O$ emission over that of a reference mature forest. This form of the response functions can effectively reproduce the short-lived increase in soil $N_2O$ emissions after

initial forest clearing and the gradually declining emission rates of converted crops/pastures[21,76]. Using these two curves and the baseline, we kept track of the $N_2O$ reduction of tropical forests and the post-deforestation crop/pasture $N_2O$ emissions at an annual time-scale. This book-keeping method was applied to the two deforestation area datasets (Supplementary Text 2.8), so we could investigate not only the difference caused by the two sets of land use data but also the difference between this empirical method and the process-based model. For land conversion from natural vegetation to croplands or pastures, DLEM uses a similar strategy to Houghton et al.[72] and McGuire et al.[77] to simulate its influences on carbon and N cycles. Moreover, through using the sites of field observation from Davidson et al.[20] and Keller and Reiners[75], we estimated $N_2O$ emission from secondary tropical forests based on the algorithm: $y = 0.0084x + 0.2401$ ($R^2 = 0.44$). $x$ (unit: year) indicates secondary forest age and $y$ (unitless; 0–1) indicates the ratio of secondary forest $N_2O$ emission over that of a reference mature forest. The difference between primary forests and secondary forests were subtracted from natural soil emissions simulated by six terrestrial biosphere models in NMIP.

We calculated the ensemble of oceanic $N_2O$ emission based on the BU approach (five ocean biogeochemical models; Supplementary Table 18) and the TD approach (five estimates from four inversion models; Supplementary Table 19), respectively. The atmospheric burden and its rate of change during 1980–2016 were derived from mean maritime surface mixing ratios of $N_2O$ (refs. [78,79]) with a conversion factor of 4.79 Tg N/ppb (ref. [80]). Combining uncertainties in measuring the mean surface mixing ratios[78] and that of converting surface mixing ratios to a global mean abundance[80], we estimate a ±1.4% uncertainty in the burden. Annual change in atmospheric abundance is calculated from the combined NOAA and AGAGE record of surface $N_2O$ and uncertainty is taken from the IPCC AR5 (ref. [2]). There shows an agreement of the

744 stratospheric loss from atmospheric chemistry transport models (TD modeled chemical sink[18,81])
745 and from satellite observations with a photolysis model (observed photochemical sink[1]), which
746 differ only by ~1 Tg N $yr^{-1}$. The satellite-based lifetime, 116±9 years, gives an overall
747 uncertainty in the annual loss of ±8%. The tropospheric loss of $N_2O$ from reaction with $O(^1D)$ is
748 included in observed atmospheric chemical sink (Table 1) and is small (~1% of the stratospheric
749 sink) with an estimated range of 0.1 to 0.2 Tg N $yr^{-1}$.

750 **Comparison with the IPCC guidelines**. The IPCC has provided guidance to quantify $N_2O$
751 emissions, which is widely used in emission inventories for reporting to the UNFCCC. Over time
752 the recommended approaches have changed, which is critical for estimating emissions from
753 agricultural soils, the largest emission source. Previous global $N_2O$ assessments[52,82,83] based on
754 the IPCC 1996 guidelines[84] attributed about 6.3 Tg N $yr^{-1}$ to the agricultural sector, including
755 both direct and indirect emissions. This estimate is significantly larger than our results (Fig. 1;
756 Table 1) derived from multiple methods, and is also larger than the most recent estimates from
757 global inventories (EDGAR v4.3.2, FAOSTAT, and GAINS) that are based on the IPCC 2006
758 guidelines[14]. The main reason is that indirect emissions from leaching and groundwater were
759 overestimated in previous studies[85]. Correspondingly, projections of atmospheric $N_2O$
760 concentrations based on these overestimated emissions[82] led to biased estimates. For example,
761 Mosier and Kroeze[82] expected atmospheric $N_2O$ concentrations to be 340–350 ppb in the year
762 2020, instead of 333 ppb[5] as observed. Recently, the 2019 Refinement to the 2006 IPCC
763 Guidelines for National Greenhouse Gas Inventories has been published. It adopts the same
764 approach for N application on soils, but considers impacts of different climate regimes. The new
765 guidelines, based on a wealth of new scientific literature, proposed much smaller emissions from
766 grazing animals by a factor of 5–7. Preliminary calculations we have made indicate that global

767 soil emissions based on these new guidelines may decrease by 20%–25%. Integrating estimates
768 relying on the IPCC methodology with estimates by process-based models provides for a more
769 balanced assessment in this paper. We also added information from assessments[86,87] that derived
770 agricultural emissions as the difference between atmospheric terms and other emissions like
771 combustion, industry and nature, and they gave comparable magnitudes (4.3–5.8 Tg N $yr^{-1}$) to
772 our bottom-up results.
773 **Uncertainty.** Current data analysis and synthesis of long-term $N_2O$ fluxes are based on a wide
774 variety of TD and BU methods. TD approaches, consisting of four inversion frameworks[88-91],
775 provide a wide range of estimates largely due to systematic errors in the modelled atmospheric
776 transport and stratospheric loss of $N_2O$. In addition, the emissions from TD analyses are
777 dependent on the magnitude and distribution of the prior flux estimates to an extent that is
778 strongly determined by the number of atmospheric $N_2O$ measurements[18]. Inversions are
779 generally not well constrained (and thus rely heavily on a priori estimates) in Africa, Southeast
780 Asia, southern South America, and over the oceans, owing to the paucity of observations in these
781 regions. The improvement of atmospheric transport models, more accurate priors, and more
782 atmospheric $N_2O$ measurements would reduce uncertainty in further TD estimates, particularly
783 for ocean and regional emissions.
784 BU approaches are subject to uncertainties in various sources from land[16] and oceans[32]. For
785 process-based models (e.g. NMIP and ocean biogeochemical models), the uncertainty is
786 associated with differences in model configuration as well as process parameterization[16,32]. The
787 uncertainty of estimates from NMIP could be reduced in multiple ways[16]. First, the six models in
788 NMIP exhibited different spatial and temporal patterns of $N_2O$ emissions even though they used
789 the same forcings. Although these models have considered essential biogeochemical processes in

790 soils (e.g., biological N fixation, nitrification/denitrification, mineralization/immobilization,
791 etc.)[92], some missing processes such as freeze-thaw cycles and ecosystem disturbances should be
792 included in terrestrial biosphere models to reduce uncertainties. Second, the quality of input
793 datasets, specifically the amount and timing of N application, and spatial and temporal changes
794 in distribution of natural vegetation and agricultural land, is critical for accurately simulating soil
795 $N_2O$ emissions. Third, national and global $N_2O$ flux measurement networks[17] could be used to
796 validate model performance and constrain large-scale model simulations. Data assimilation
797 techniques could be utilized to improve model accuracy.
798 Current remaining uncertainty in global ocean model estimates of $N_2O$ emission includes the
799 contribution of $N_2O$ flux derived from the tropical oceanic low oxygen zones (e.g., the Eastern
800 Equatorial Pacific, the northern Indian ocean) relative to the global ocean. These low oxygen
801 zones are predominantly influenced by high yield $N_2O$ formation processes (e.g., denitrification
802 and enhanced nitrification). Regional observation-based assessments have also suggested that
803 these regions may produce more $N_2O$ than is simulated by the models[32]. The current generation
804 of global ocean biogeochemistry models are not sufficiently accurate to represent the high $N_2O$
805 production processes in low-oxygen zones, and their associated variability (see refs. [34,93,94] for
806 more detail). Thus, precisely representing the local ocean circulation and associated
807 biogeochemical fluxes of these regions could further reduce the uncertainty in estimates of
808 global and regional oceanic $N_2O$ emissions.
809 Regardless of the tier approach used, GHG inventories for agriculture suffer from high
810 uncertainty in the underlying agriculture and rural data and statistics used as input, including
811 statistics on fertilizer use, livestock manure availability, storage and applications, and nutrient,
812 crop and soils management. For instance, animal waste management is an uncertain aspect, since

much of the manure is either not used, or employed as a fuel or building material, or may be discharged directly to surface water[95,96], with important repercussions for the calculated emissions. Furthermore, GHG inventories using default EFs show large uncertainties at local to global scales, especially for agricultural $N_2O$ emissions, due to the poorly captured dependence of EFs on spatial diversity in climate, management, and soil physical and biochemical conditions[2,22]. It is well known, for example from the IPCC guidelines, that higher-tier GHG inventories may provide more reasonable estimates by using the alternative EFs that are disaggregated by environmental factors and management-related factors[97]. A large range of EFs have been used to estimate aquaculture $N_2O$ emissions[31,39,62,86] and long-term estimates of N flows in freshwater and marine aquaculture are scarce[30]. Uncertainty also remains in several $N_2O$ sources that have not yet been fully understood or quantified. To date, robust estimates of $N_2O$ emissions from global peatland degradation are still lacking, although we have accounted for $N_2O$ emissions due to the drainage of organic soils (histosols) obtained from FAOSTAT and GAINS databases[28,43]. Recent evidence shows that permafrost thawing[98] and the freeze-thaw cycle[99] contribute to increasing $N_2O$ emissions, which, however, have not been well established in the current estimates of the global $N_2O$ budget.

**Statistics.** Through using the Mann-Kendall test in R-3.4.4, we checked the significance of trends in annual $N_2O$ emissions from each sub-sector based on the BU approach.

## References


50 Nevison, C. D., Lueker, T. J. & Weiss, R. F. Quantifying the nitrous oxide source from coastal upwelling. *Global Biogeochemical Cycles* **18**, GB1018 (2004).

51 Lauerwald, R. *et al.* Natural lakes are a minor global source of $N_2O$ to the atmosphere. *Global Biogeochemical Cycles* **33**, 1564-1581 (2019).

52 Kroeze, C., Mosier, A. & Bouwman, L. Closing the global $N_2O$ budget: a retrospective analysis 1500–1994. *Global Biogeochemical Cycles* **13**, 1-8 (1999).

53 Schumann, U. & Huntrieser, H. The global lightning-induced nitrogen oxides source. *Atmospheric Chemistry and Physics* **7**, 3823-3907 (2007).

54 De Klein, C. *et al.* $N_2O$ emissions from managed soils, and $CO_2$ emissions from lime and urea application. *IPCC Guidelines for National Greenhouse Gas Inventories, Prepared by the National Greenhouse Gas Inventories Programme* **4**, 1-54 (2006).

55 Dentener, F. J. & Crutzen, P. J. A three-dimensional model of the global ammonia cycle. *Journal of Atmospheric Chemistry* **19**, 331-369 (1994).

56 Röckmann, T., Kaiser, J., Crowley, J. N., Brenninkmeijer, C. A. & Crutzen, P. J. The origin of the anomalous or "mass-independent" oxygen isotope fractionation in tropospheric $N_2O$. *Geophysical Research Letters* **28**, 503-506 (2001).

57 Kaiser, J. & Röckmann, T. Absence of isotope exchange in the reaction of $N_2O+O(^1D)$ and the global $\Delta^{17}O$ budget of nitrous oxide. *Geophysical Research Letters* **32** (2005).

58 Schlesinger, W. H. An estimate of the global sink for nitrous oxide in soils. *Global Change Biology* **19**, 2929-2931 (2013).

59 Syakila, A., Kroeze, C. & Slomp, C. P. Neglecting sinks for $N_2O$ at the earth's surface: does it matter? *Journal of Integrative Environmental Sciences* **7**, 79-87 (2010).

60 Bouwman, A. F. *et al.* Hindcasts and future projections of global inland and coastal nitrogen and phosphorus loads due to finfish aquaculture. *Reviews in Fisheries Science* **21**, 112-156 (2013).

61 Bouwman, A. F. *et al.* Global hindcasts and future projections of coastal nitrogen and phosphorus loads due to shellfish and seaweed aquaculture. *Reviews in Fisheries Science* **19**, 331-357 (2011).

62 Hu, Z., Lee, J. W., Chandran, K., Kim, S. & Khanal, S. K. Nitrous oxide ($N_2O$) emission from aquaculture: a review. *Environmental science technology* **46**, 6470-6480 (2012).

63 Williams, J. & Crutzen, P. J. Nitrous oxide from aquaculture. *Nature Geoscience* **3**, 143 (2010).

64 Andela, N. *et al.* A human-driven decline in global burned area. *Science* **356**, 1356-1362 (2017).

65 Yang, J. *et al.* Spatial and temporal patterns of global burned area in response to anthropogenic and environmental factors: Reconstructing global fire history for the 20th and early 21st centuries. *Journal of Geophysical Research: Biogeosciences* **119**, 249-263 (2014).

66 Dennis, R. A review of fire projects in Indonesia (1982-1998). *Cifor* (1999).

67 Suntharalingam, P. *et al.* Quantifying the impact of anthropogenic nitrogen deposition on oceanic nitrous oxide. *Geophysical Research Letters* **39**, L07605 (2012).

68 Murray, R. H., Erler, D. V. & Eyre, B. D. Nitrous oxide fluxes in estuarine environments: response to global change. *Global Change Biology* **21**, 3219-3245 (2015).

69 Erler, D. V. *et al.* Applying cavity ring‐down spectroscopy for the measurement of dissolved nitrous oxide concentrations and bulk nitrogen isotopic composition in aquatic systems: Correcting for interferences and field application. *Limnology and Oceanography: Methods* **13**, 391-401 (2015).

70 Murray, R., Erler, D., Rosentreter, J. & Eyre, B. Seasonal and spatial $N_2O$ concentrations and emissions in three tropical estuaries. *Marine Chemistry* 221, 103779 (2020).

71 Vernberg, F. J. & Vernberg, W. B. *The coastal zone: past, present, and future*. Univ of South Carolina Press (2001).

72 Houghton, R. *et al.* Changes in the Carbon Content of Terrestrial Biota and Soils between 1860 and 1980: A Net Release of $CO_2$ to the Atmosphere. *Ecological monographs* **53**, 235-262 (1983).
73 Davidson, E. A. The contribution of manure and fertilizer nitrogen to atmospheric nitrous oxide since 1860. *Nature Geoscience* **2**, 659-662 (2009).
74 van Lent, J., Hergoualc'h, K. & Verchot, L. V. Reviews and syntheses: Soil $N_2O$ and NO emissions from land use and land-use change in the tropics and subtropics: a meta-analysis. *Biogeosciences* **12**, 7299-7313 (2015).
75 Keller, M. & Reiners, W. A. Soil-atmosphere exchange of nitrous oxide, nitric oxide, and methane under secondary succession of pasture to forest in the Atlantic lowlands of Costa Rica. *Global Biogeochemical Cycles* **8**, 399-409 (1994).
76 Melillo, J. M. *et al.* Nitrous oxide emissions from forests and pastures of various ages in the Brazilian Amazon. *Journal of Geophysical Research: Atmospheres* **106**, 34179-34188 (2001).
77 McGuire, A. *et al.* Carbon balance of the terrestrial biosphere in the twentieth century: Analyses of $CO_2$, climate and land use effects with four process-based ecosystem models. *Global Biogeochemical Cycles* **15**, 183-206 (2001).
78 Dlugokencky, E., Steele, L., Lang, P. & Masarie, K. The growth rate and distribution of atmospheric methane. *Journal of Geophysical Research: Atmospheres* **99**, 17021-17043 (1994).
79 Prather, M. *et al.* Annex II: Climate system scenario tables. *Cambridge, United Kingdom and New York, NY, USA* (2013).
80 Prather, M. J., Holmes, C. D. & Hsu, J. Reactive greenhouse gas scenarios: Systematic exploration of uncertainties and the role of atmospheric chemistry. *Geophysical Research Letters* **39**, L09803 (2012).
81 Prather, M. J. & Hsu, J. Coupling of Nitrous Oxide and Methane by Global Atmospheric Chemistry. *Science* **330**, 952-954 (2010).
82 Mosier, A. & Kroeze, C. Potential impact on the global atmospheric $N_2O$ budget of the increased nitrogen input required to meet future global food demands. *Chemosphere-Global Change Science* **2**, 465-473 (2000).
83 Mosier, A. *et al.* Closing the global $N_2O$ budget: nitrous oxide emissions through the agricultural nitrogen cycle. *Nutrient cycling in Agroecosystems* **52**, 225-248 (1998).
84 IPCC. Revised 1996 IPCC guidelines for national greenhouse gas inventories. *Hayama, Japan* (1997).
85 Nevison, C. in IPCC, Background Papers: IPCC Expert Meetings on Good Practice Guidance and Uncertainty Management in National Greenhouse Gas Inventories. *IPCC National Greenhouse Gas Inventories Programme, Technical Support Unit.* 381-397 (2000).
86 Crutzen, P. J., Mosier, A. R., Smith, K. A. & Winiwarter, W. $N_2O$ release from agro-biofuel production negates global warming reduction by replacing fossil fuels. *Atmospheric Chemistry and Physics* **8**, 389-395 (2008).
87 Smith, K. A., Mosier, A. R., Crutzen, P. J. & Winiwarter, W. The role of $N_2O$ derived from crop-based biofuels, and from agriculture in general, in Earth's climate. *Philosophical Transactions of the Royal Society of London B: Biological Sciences* **367**, 1169-1174 (2012).

88 Thompson, R. L. *et al.* Nitrous oxide emissions 1999 to 2009 from a global atmospheric inversion. *Atmospheric Chemistry and Physics* **14**, 1801-1817 (2014).
89 Wells, K. C. *et al.* Simulation of atmospheric $N_2O$ with GEOS-Chem and its adjoint: evaluation of observational constraints. *Geoscience Model Development* **8**, 3179-3198 (2015).
90 Wilson, C., Chipperfield, M., Gloor, M. & Chevallier, F. Development of a variational flux inversion system (INVICAT v1. 0) using the TOMCAT chemical transport model. *Geoscientific Model Development* **7**, 2485-2500 (2014).
91 Patra, P. K. *et al.* Improved Chemical Tracer Simulation by MIROC4. 0-based Atmospheric Chemistry-Transport Model (MIROC4-ACTM). *Sola* **14**, 91-96 (2018).
92 Tian, H. Q. *et al.* The Global $N_2O$ Model Intercomparison Project. *Bulletin of the American Meteorological Society* **99**, 1231-1252 (2018).
93 Suntharalingam, P. *et al.* Anthropogenic nitrogen inputs and impacts on oceanic $N_2O$ fluxes in the northern Indian Ocean: The need for an integrated observation and modelling approach. *Deep Sea Research Part II: Topical Studies in Oceanography* **166**, 104-113 (2019).
94 Battaglia, G. & Joos, F. Marine $N_2O$ Emissions From Nitrification and Denitrification Constrained by Modern Observations and Projected in Multimillennial Global Warming Simulations. *Global Biogeochemical Cycles* **32**, 92-121 (2018).
95 Galloway, J. *et al.* The impact of animal production systems on the nitrogen cycle. Vol. 1, *Island Press* (2010).
96 Steinfeld, H., Mooney, H. A., Schneider, F. & Neville, L. E. Livestock in a changing landscape, volume 1: drivers, consequences, and responses. Vol. 1, *Island Press* (2013).
97 IPCC. 2019 Refinement to the 2006 IPCC Guidelines for National Greenhouse Gas Inventories. *Hayama, Japan* (2019).
98 Elberling, B., Christiansen, H. H. & Hansen, B. U. High nitrous oxide production from thawing permafrost. *Nature Geoscience* **3**, 332-335 (2010).
99 Wagner-Riddle, C. *et al.* Globally important nitrous oxide emissions from croplands induced by freeze–thaw cycles. *Nature Geoscience* **10**, 279-283 (2017).
100 Suntharalingam, P. *et al.* Estimates of Oceanic Nitrous-oxide Emissions from Global Biogeochemistry Models. *American Geophysical Union, Fall Meeting 2018* (2018).
101 Janssens-Maenhout, G. *et al.* EDGAR v4.3.2 Global Atlas of the three major greenhouse gas emissions for the period 1970–2012. *Earth System Science Data* **11**, 959-1002 (2019).
102 Tubiello, F. *et al.* Estimating greenhouse gas emissions in agriculture: a manual to address data requirements for developing countries. *FAO, Rome* (2015).
103 Van Der Werf, G. R. *et al.* Global fire emissions estimates during 1997-2016. *Earth System Science Data* **9**, 697-720 (2017).
104 Dentener, F. Global maps of atmospheric nitrogen deposition, 1860, 1993, and 2050. *Data set. Available on-line (http://daac. ornl. gov/) from Oak Ridge National Laboratory Distributed Active Archive Center, Oak Ridge, TN, USA* (2006).
105 Riahi, K. *et al.* The Shared Socioeconomic Pathways and their energy, land use, and greenhouse gas emissions implications: An overview. *Global Environmental Change* **42**, 153-168 (2017).

**Data availability**

The relevant datasets of this study are archived in the box site of International Center for Climate and Global Change Research at Auburn University (https://auburn.box.com/). Source data for Figs. 1–4, Table 1, Extended Figs. 1–10 and Supplementary Information are provided with the paper. Additional description on data availability for atmospheric $N_2O$ observations from NOAA, AGAGE and CSIRO networks is provided in the Supplementary Information. The data presented here are made available in the belief that their dissemination will lead to greater understanding and new scientific insights on the global and regional $N_2O$ budgets and changes to it, and helping to reduce the uncertainties. As data are the result of initial processing to fit to the purpose of this publication, typically a wealth of underlying information is with the original data providers. Researchers interested to use results made available in the repository are encouraged, as good practice, to take advantage of underlying information by contacting the original data providers. If such a contact develops into a more intensive scientific discussion, further involvement including co-authorship should be considered.

## Code availability

The relevant codes of this study are archived in the box site of International Center for Climate and Global Change Research at Auburn University (https://auburn.box.com/).

## Acknowledgements

This paper is the result of a collaborative international effort under the umbrella of the Global Carbon Project (a project of Future Earth and a research partner of the World Climate Research Programme) and International Nitrogen Initiative. This research was made possible partly by Andrew Carnegie Fellowship Award no. G-F-19-56910; NSF grant nos. 1903722,1243232 and 1922687; NASA grant nos. NNX14AO73G, NNX10AU06G, NNX11AD47G and NNX14AF93G; NOAA grant nos. NA16NOS4780207 and NA16NOS4780204; National Key R & D Program of China (grant nos. 2017YFA0604702 and 2018YFA0606001), National Natural Science Foundation of China (Grant no. 41961124006), CAS grants (KFJ-STSZDTP-0; SKLURE2017-1-6), and OUC-AU Joint Center Program. Additional funding support includes: E.T.B, P.R., G.P.P., R.L.T., P.S. acknowledge funding support from VERIFY project (EC H2020 grant no. 776810). P.S. also acknowledges funding from the EC H2020 grant No 641816 (CRESCENDO); A.I. acknowledges funding support from JSPS KAKENHI grant (no. 17H01867). G.B., F.J, and S.L. acknowledge support by Swiss National Science Foundation (#200020_172476) and by the EC H2020 grant no. 821003 (Project 4C) and no. 820989 (Project COMFORT). A.L. acknowledges support by DFG project SFB754/3. S.Z. acknowledges support by the EC H2020 grant no. 647204. K.C.W. and D.B.M. acknowledge support from NASA (IDS Grant #NNX17AK18G) and NOAA (Grant #NA13OAR4310086); P.A.R. acknowledges NASA Award NNX17AI74G, M.M. acknowledges support from the Scottish Government's Rural and Environment Science and Analytical Services Division (RESAS) Environmental Change Programme (2016-2021); B.E. acknowledges the support from ARC Linkage Grants LP150100519 and LP190100271; M.P. acknowledges US Department of Energy, DE-SC0012536; Lawrence Livermore National Laboratory, B628407 and NASA MAP program, NNX13AL12G; S.B. was supported by the EC H2020 with the CRESCENDO project (grant no. 641816) and by the COMFORT project (grant no. 820989). S.B. also acknowledges the support of the team in charge of the CNRM-CM climate model; F.Z. acknowledges the support from the

National Natural Science Foundation of China (41671464). Supercomputing time was provided by the Météo-France/DSI supercomputing center. P.K.P. is partly supported by Environment Research and Technology Development Fund (#2-1802) of the Ministry of the Environment, Japan. R.L. acknowledges support from the French state aid managed by the ANR under the "Investissements d'avenir" programme with the reference ANR-16-CONV-0003. NOAA ground-based observations of atmospheric $N_2O$ are supported by NOAA's Climate Program Office under the Atmospheric Chemistry Carbon Cycle and Climate (AC4) theme. The AGAGE stations measuring $N_2O$ are supported by NASA (USA) grants NNX16AC98G to MIT, and NNX16AC97G and NNX16AC96G to SIO, and by BEIS (UK) for Mace Head, NOAA (USA) for Barbados, and CSIRO and BoM (Australia) for Cape Grim. We also thank Dr. Steve Frolking and two anonymous reviewers for constructive comments and suggestions that have helped improve this paper. The statements made and views expressed are solely the responsibility of the authors.

## Author contributions

Author contributions. H.T., R.L.T., J.G.C. and R.B.J. designed and coordinated the study. H.T., R.X., J.G.C., R.L.T., W.W., P.S., E.A.D., P.C., R.B.J., G.J.M., M.J.P., N.P., S.P., P.R., H.S., F.N.T., S.Z., F.Z., B.F. and G.P. conducted data analysis, synthesis and wrote the paper. R.L.T. led atmospheric inversions teaming with M.P.C., T.M., D.B.M., P.K.P., K.C.W., and C.W.; H.T. led land biosphere modeling teaming with P.C., H.S., S.Z., A.A., F.J., J.C., S.R.S.D., A.I., W.L., S.L., S.O., N.V., E.A.D., S.D. and W. Li; P.S. led ocean biogeochemical modeling teaming with G.B., L.B., S.B., E.T.B., F.J. and A.L.; P.R. led inland water and coastal modeling and synthesis teaming with B.D.E., G.G.L., R.L., T.M., P.A.R., H.T. and Y.Y.; A.F.B., J.W., M.M. provided data of $N_2O$ flux in aquaculture. G.R.W. and J.Y. provided data of $N_2O$ emissions from biomass burning. F.Z. provided cropland $N_2O$ flux data from a statistical model and field observations. G.J.M., F.N.T. and W.W. provided $N_2O$ inventory data. M.J.P. and D.J.R. provided data of stratospheric and tropospheric sinks. G.P.P. provided RCP and SSP scenarios data and analysis. B.H., E.D. and J.E. provided a global $N_2O$ monitoring dataset of NOAA/ESRL GMD. R.P. and R.W. provided a global $N_2O$ monitoring dataset of AGAGE stations. P.K. provided a global $N_2O$ monitoring dataset of CSIRO. All coauthors reviewed and commented on the manuscript.

**Competing interests: The authors declare no competing interests.**

## Additional information

**Supplementary information is available for this paper at https://**

**Correspondence and requests for materials should be addressed to H.T.**

tianhan@auburn.edu

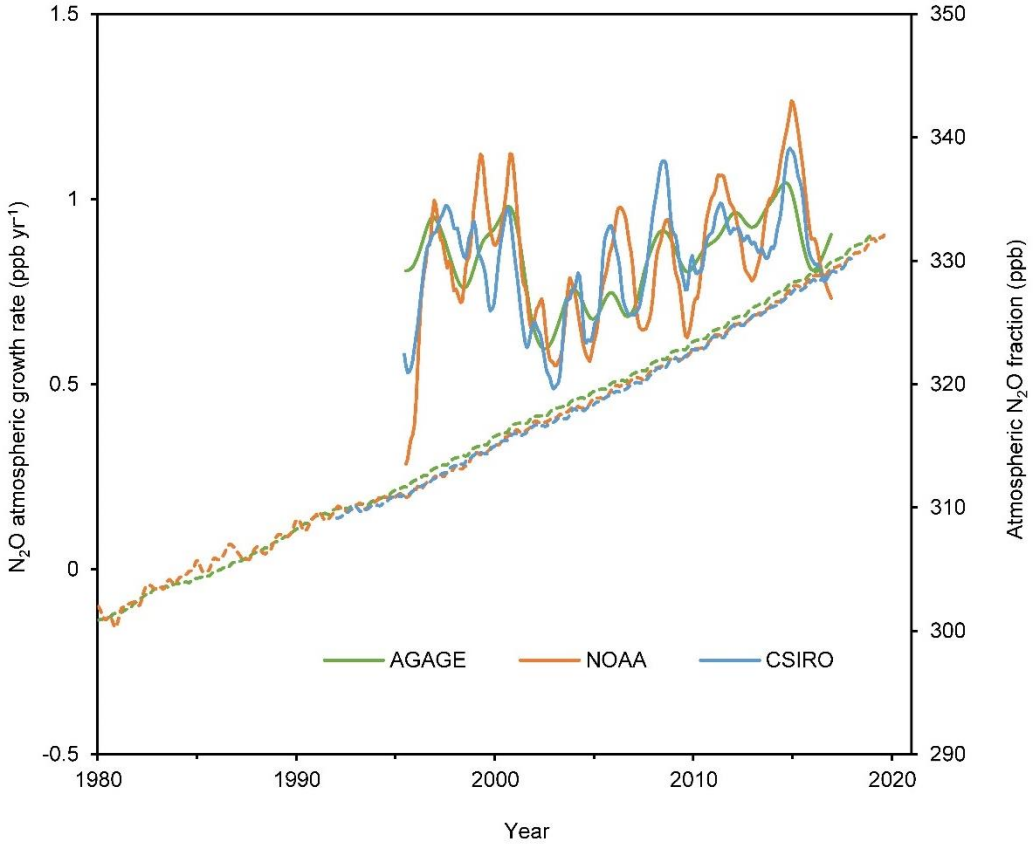


**Extended Data Fig. 1 Global mean growth rates and atmospheric concentration of $N_2O$.** Global mean growth rates (solid lines, during 1995–2017) and atmospheric $N_2O$ concentration (dashed lines, during 1980–2017) are from the AGAGE[6] (green), NOAA[5] (orange), and CSIRO (blue) networks. Global mean growth rates were calculated with annual time steps and are shown as 12-month moving averages. Growth rates are not calculated prior to 1995 due to insufficient data and higher uncertainties on the measurements.

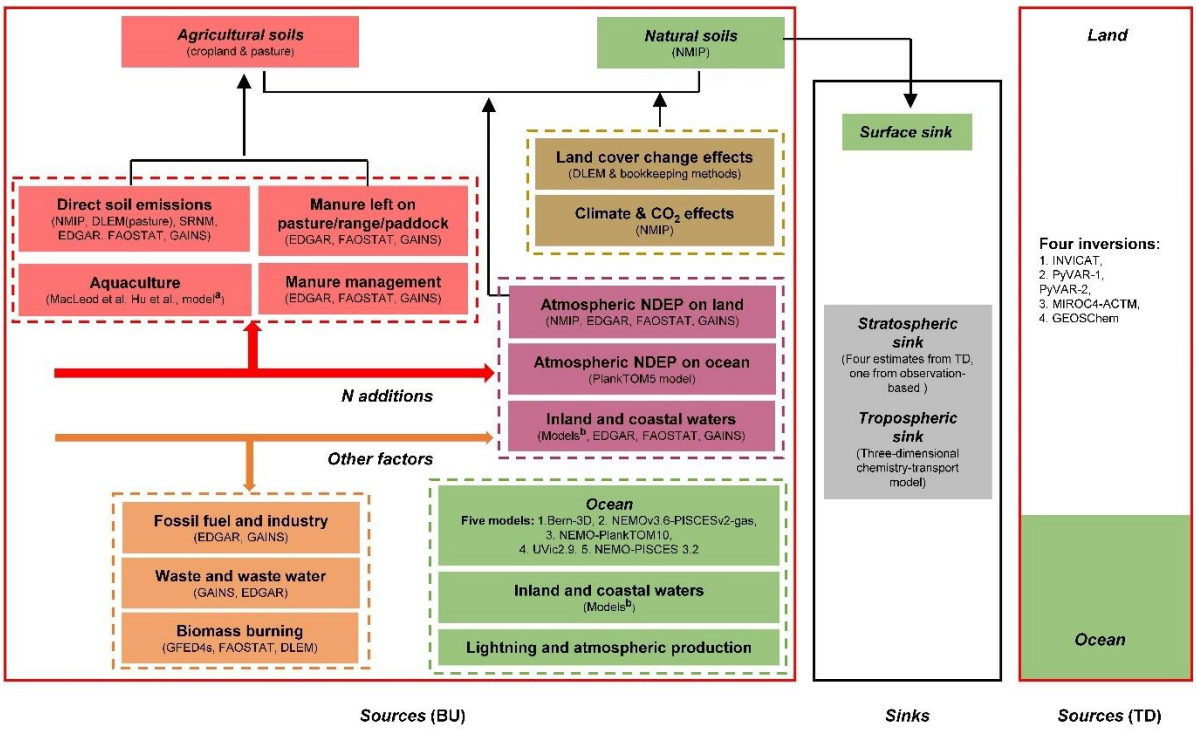


**Extended Data Fig. 2 The methodology for data synthesis of global $N_2O$ budget.** BU and TD represent bottom-up and top-down methods, respectively. The color codes are the same as that used in Table 1 and Figs. 1–3. We utilize both approaches, including 22 BU and five TD estimates of $N_2O$ fluxes from land and oceans. For sources estimated by BU, we include six process-based terrestrial biosphere modeling studies[16]; five process-based ocean biogeochemical models[100]; one nutrient budget model[30,60,61]; five inland water modeling studies[35,36,50,51,68]; one statistical model SRNM based on spatial extrapolation of field measurements[17]; and four GHG inventories: EDGAR v4.3.2[101], FAOSTAT[102], GAINS[43], and GFED4s[103]. In addition, previous literatures regarding estimates of 'Surface sink'[58,73], 'Lightning'[53,54], 'Atmospheric production'[56,57,104], 'Aquaculture'[31,62], and model-based 'Tropospheric sink'[81] and observed 'Stratospheric sink'[1] are included in the current synthesis. [a]MacLeod et al.[31] and Hu et al.[62] provide global aquaculture $N_2O$ emissions in 2013 and in 2009, respectively; and the nutrient budget model[30,60,61] provides N flows in global freshwater and marine aquaculture over the period 1980–2016. [b]Model-based estimates of $N_2O$ emissions from 'Inland and coastal waters' include rivers and reservoirs[35,36], lakes[51], estuaries[35], coastal zones (i.e., seagrasses, mangroves, saltmarsh and intertidal saltmarsh)[68], and coastal upwelling[50].

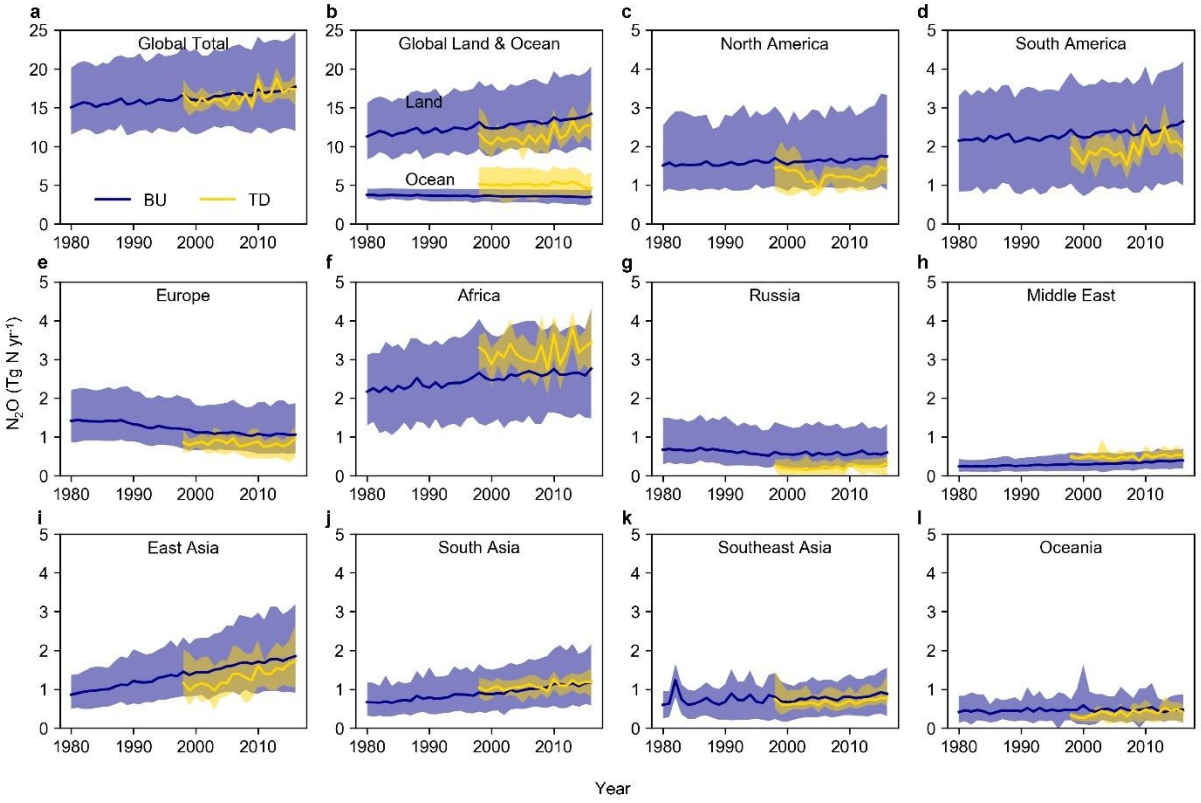


**Extended Data Fig. 3 Comparison of annual total $N_2O$ emissions at global and regional scales estimated by BU and TD approaches.** The blue lines represent the mean $N_2O$ emission from BU methods and the shaded areas show minimum and maximum estimates; The gold lines represent the mean $N_2O$ emission from TD methods and the shaded areas show minimum and maximum estimates.

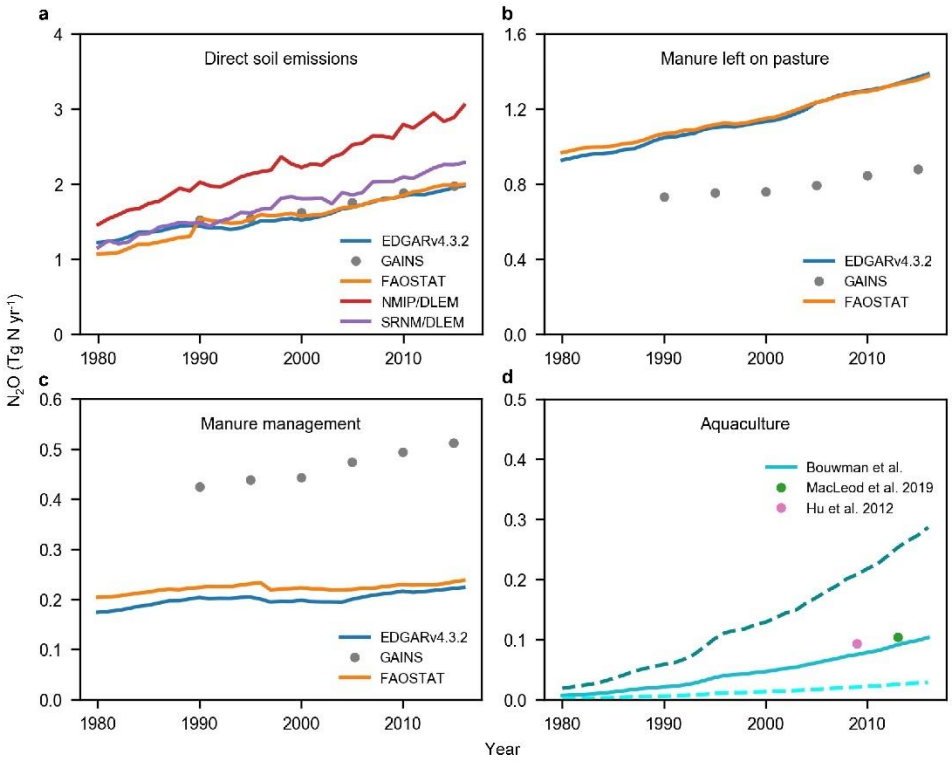


**Extended Data Fig. 4 Global agricultural $N_2O$ emissions. a,** Direct emission from agricultural soils associated with mineral fertilizer, manure and crop residue inputs, and cultivation of organic soils based on EDGAR v4.3.2, GAINS, FAOSTAT, NMIP/DLEM, and SRNM/DLEM estimates. NMIP/DLEM or SRNM/DLEM means the combination of $N_2O$ emission by NMIP or SRNM from croplands with $N_2O$ emission from intensively managed grassland (pasture) by DLEM. **b,** Direct emission from the global total area under permanent meadows and pasture, due to manure N deposition (left on pasture) based on EDGAR v4.3.2, FAOSTAT, and GAINS estimates. **c,** Emission from manure management based on FAOSTAT, GAINS, and EDGAR v4.3.2. **d,** Aquaculture $N_2O$ emission based on a nutrient budget model[30], MacLeod et al.[31], and Hu et al.[62]; the solid line represents the 'best estimate' that is the product of EF (1.8%) and N waste from aquaculture provided by the nutrient budget model; the dashed lines represent the minimum and maximum values.

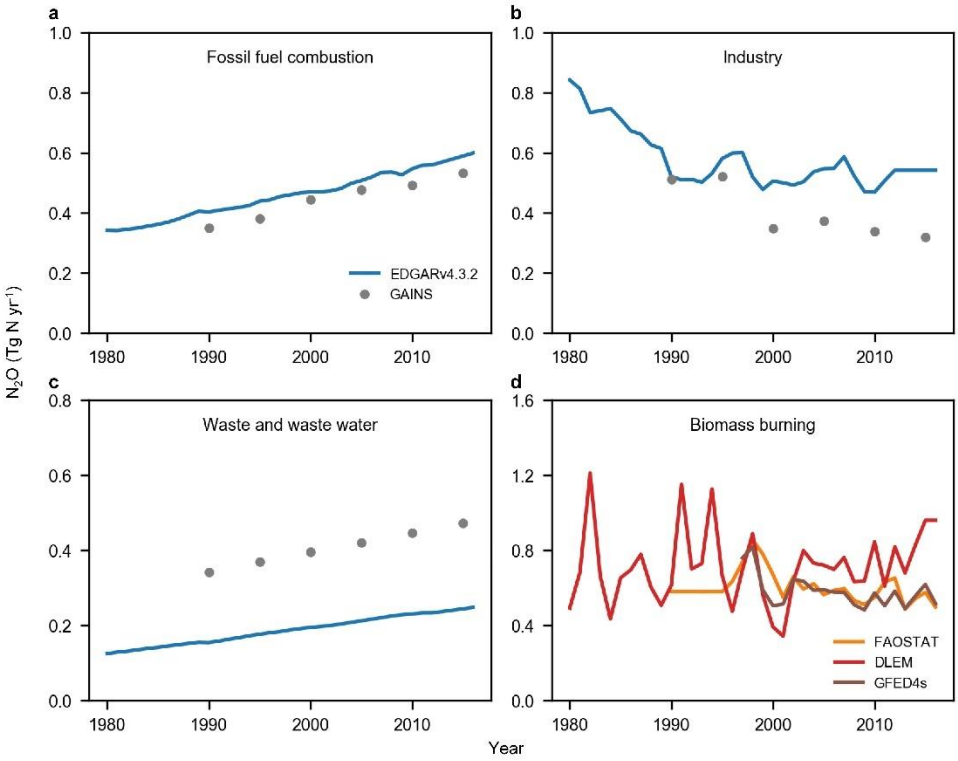


**Extended Data Fig. 5 Global $N_2O$ emission from other direct anthropogenic sources. a,** Emission from fossil fuel combustion based on EDGAR v4.3.2 and GAINS estimates. **b,** Emission from industry based on EDGAR v4.3.2 and GAINS estimates. **c,** Emission from waste and waste water based on EDGAR v4.3.2 and GAINS estimates. **d,** Emission from biomass burning based on FAOSTAT, DLEM, and GFED4s estimates.

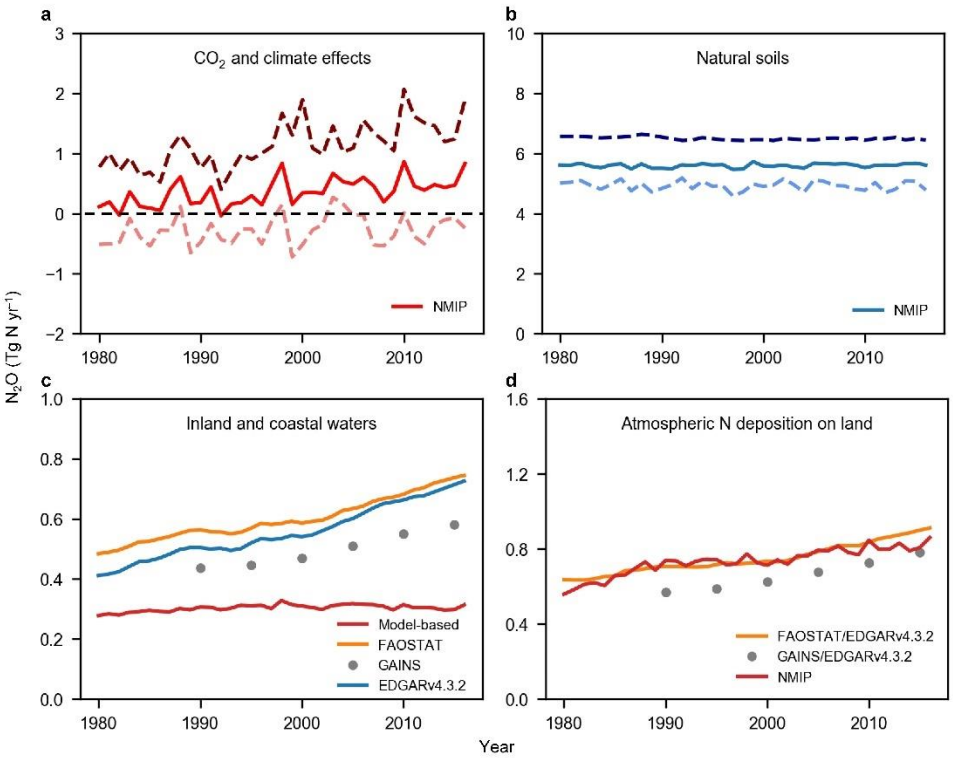


**Extended Data Fig. 6 Global $N_2O$ emissions from natural soils, inland and coastal waters and due to change in climate, atmospheric $CO_2$ and N deposition. a,** Changes in global soil $N_2O$ fluxes due to changing $CO_2$ and climate. **b,** Global natural soil $N_2O$ emissions without consideration of land use change (e.g., deforestation) and without consideration of indirect anthropogenic effects via global change (i.e., climate, elevated $CO_2$, and atmospheric N deposition). The estimates are based on NMIP estimates during 1980–2016 including six process-based land biosphere models. Here, we also subtracted the difference between with and without consideration of secondary forests emissions that grow back after pasture or cropland abandonment from natural soil emissions based on NMIP estimates. The solid lines represent the ensemble and dashed lines show the minimum and maximum values. **c,** Global anthropogenic $N_2O$ emission from inland waters, estuaries, coastal zones based on models (model-based), FAOSTAT, GAINS, and EDGAR v4.3.2 estimates. **d,** Emission due to atmospheric N deposition (NDEP) on land based on NMIP, FAOSTAT/EDGAR v4.3.2, and GAINS/EDGAR v4.3.2. FAOSTAT/EDGAR v4.3.2 or GAINS/EDGAR v4.3.2 means the combination of agricultural source from FAOSTAT or GAINS with non-agricultural source from EDGAR v4.3.2. A process-based model DLEM[36] and a mechanistic stochastic model[35,51] were used to estimate $N_2O$ emission from inland waters and estuaries, while site-level emission rates of $N_2O$ were upscaled to estimate global $N_2O$ fluxes from the global seagrass area[68].

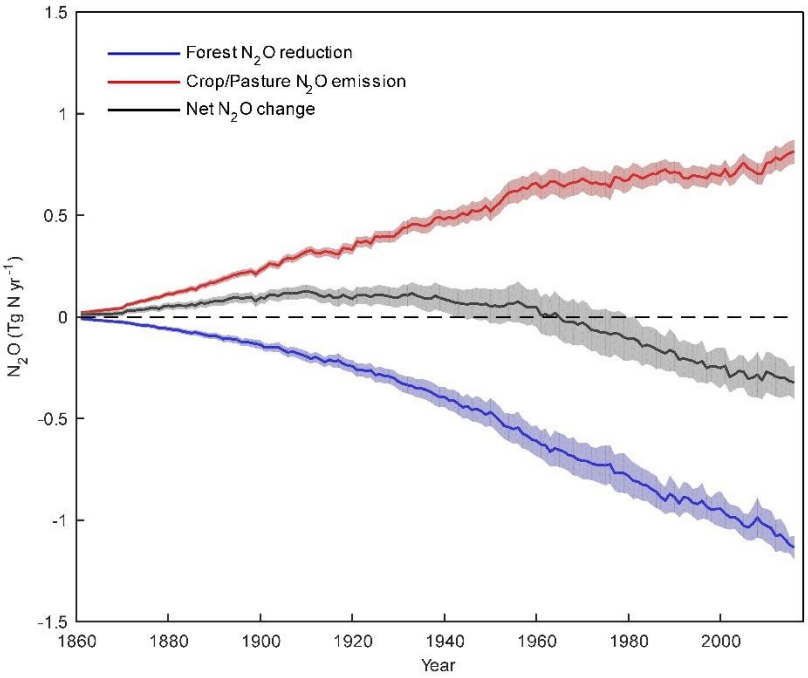


**Extended Data Fig. 7 Global $N_2O$ dynamics due to land cover changes.** The blue line represents the mean forest $N_2O$ reduction caused by the long-term effect of reduced mature forest area (i.e., deforestation) and shaded areas show minimum and maximum estimates; the red line represents the mean $N_2O$ emission from post-deforestation pulse effect (i.e., crop/pasture $N_2O$ emissions from legacy N of previous forest soil, not accounting for new fertilizer N added to these crop/pasture lands) and shaded areas show minimum and maximum estimates; the gray line represents the mean net deforestation emission of $N_2O$ and shaded areas show minimum and maximum estimates.

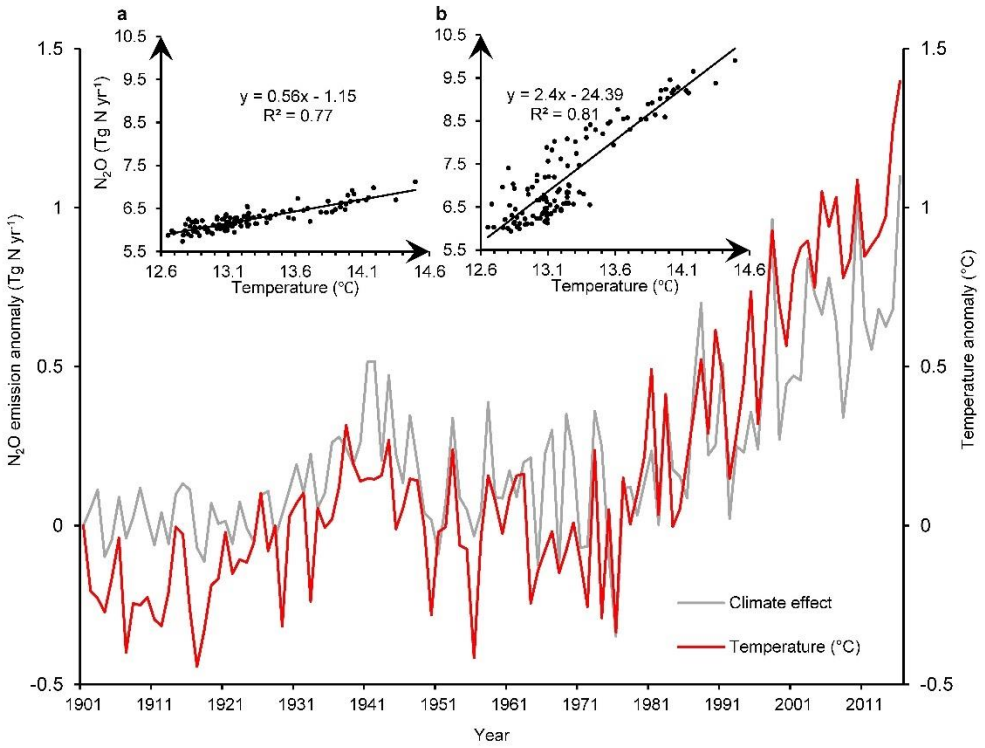


**Extended Data Fig. 8 Global simulated $N_2O$ emission anomaly due to climate effect and global annual land surface temperature anomaly during 1901–2016.** Global $N_2O$ emission anomalies are the ensemble of six process-based land biosphere models in NMIP. The temperature data were obtained from the CRU-NCEP v8 climate dataset (https://vesg.ipsl.upmc.fr). The above left figure **a)** shows the correlation between average global annual land surface temperature and simulated $N_2O$ emissions (i.e., the result of SE6 experiment in NMIP[16]) considering annual changes in climate but keeping all other factors (i.e., N fertilizer, manure, NDEP, elevated $CO_2$, and land cover change) at the level of 1860. The above right figure **b)** shows the correlation between average global annual land surface temperature and simulated $N_2O$ emissions (i.e., the result of SE1 experiment in NMIP[16]) considering annual changes in all factors during 1860–2016.

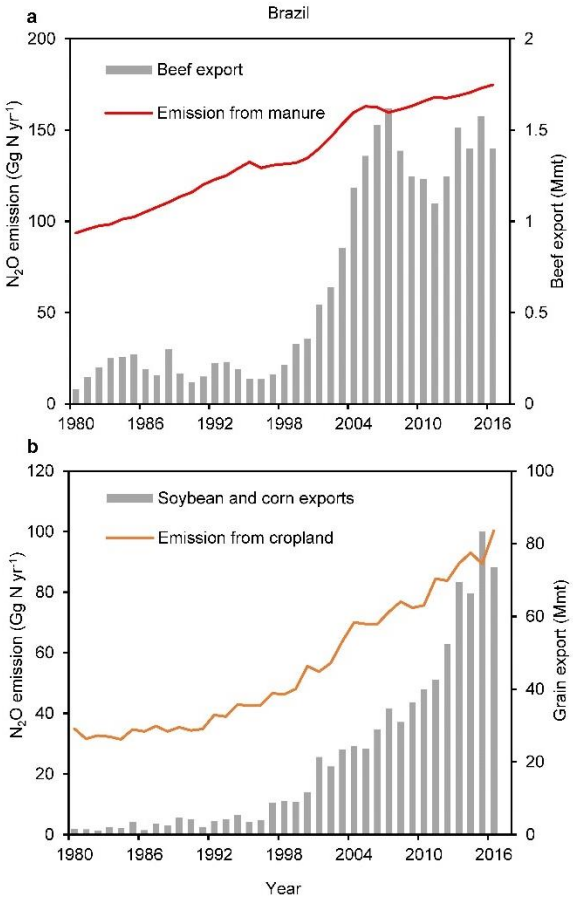


**Extended Data Fig. 9 Direct soil emissions and agricultural product trades in Brazil. a,** Red line shows the ensemble direct $N_2O$ emissions from livestock manure based on EDGAR v4.3.2, GAINS, and FAOSTAT, the sum of 'manure left on pasture' and 'manure management'; The gray columns show the amount of beef export by Brazil. **b,** Orange line shows the ensemble direct $N_2O$ emissions from croplands due to N fertilization based on NMIP and SRNM; The gray columns show the amount of soybean and corn exports by Brazil. The data of beef and cereal product trades were adapted from the ABIEC (beef) and FAOSTAT (soybean and corn). Mmt $yr^{-1}$ represents millions of metric tons per year.

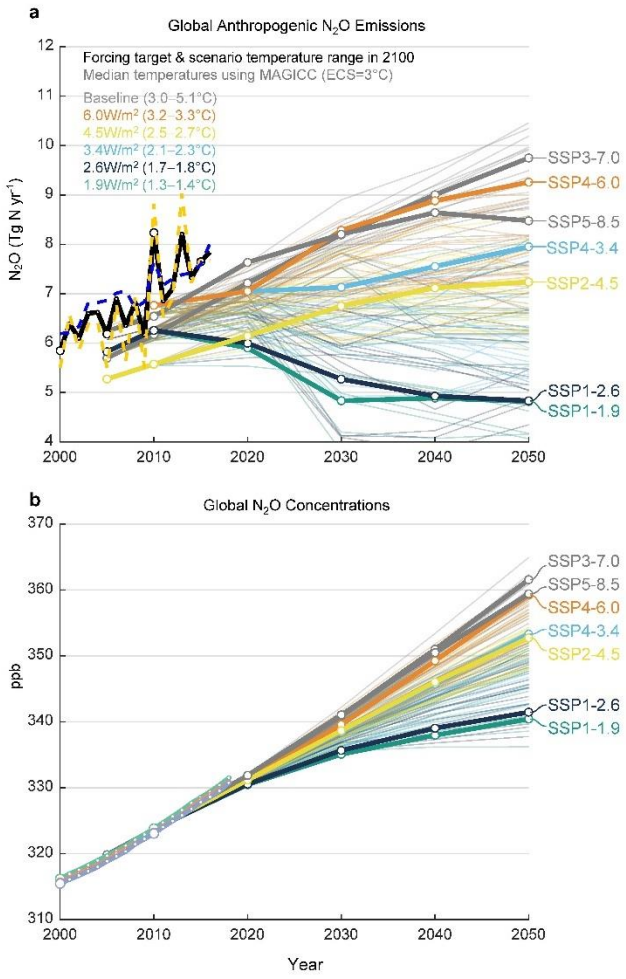


**Extended Data Fig. 10 An extension of Fig. 4 to provide a comparison of anthropogenic $N_2O$ emissions (a) and atmospheric $N_2O$ concentrations (b) in the unharmonized SSPs[105].** The emission and concentration data are as in Fig. 4. The unharmonized emissions from the Integrated Assessment Models (IAMs)[105] show a large variation due to different input data and model assumptions. Comparison with Fig. 4b, d illustrates the modifications to the IAM scenario data for use in CMIP6. All baseline scenarios (SSP3-7.0 and SSP5-8.5; without climate policy applied) are shown in gray regardless of the radiative forcing level they reach in 2100.